Article

Conformational coupling between extracellular and transmembrane domains modulates holo-adhesion GPCR function

Szymon P. Kordon [1,2,3,4,7], Kristina Cechova [5,7], Sumit J. Bandekar [1,2,3,4], Katherine Leon[1,2,3], Przemysław Dutka[1,6], Gracie Siffer [5], Anthony A. Kossiakoff [1], Reza Vafabakhsh [5] ✉ & Demet Araç [1,2,3,4] ✉

Adhesion G Protein-Coupled Receptors (aGPCRs) are key cell-adhesion molecules involved in numerous physiological functions. aGPCRs have large multidomain extracellular regions (ECRs) containing a conserved GAIN domain that precedes their seven-pass transmembrane domain (7TM). Ligand binding and mechanical force applied on the ECR regulate receptor function. However, how the ECR communicates with the 7TM remains elusive, because the relative orientation and dynamics of the ECR and 7TM within a holoreceptor is unclear. Here, we describe the cryo-EM reconstruction of an aGPCR, Latrophilin3/ADGRL3, and reveal that the GAIN domain adopts a parallel orientation to the transmembrane region and has constrained movement. Single-molecule FRET experiments unveil three slow-exchanging FRET states of the ECR relative to the transmembrane region within the holoreceptor. GAIN-targeted antibodies, and cancer-associated mutations at the GAIN-7TM interface, alter FRET states, cryo-EM conformations, and receptor signaling. Altogether, this data demonstrates conformational and functional coupling between the ECR and 7TM, suggesting an ECR-mediated mechanism for aGPCR activation.

With 33 members in humans, the adhesion G protein-coupled receptors (aGPCRs) make up the second-largest GPCR family, but the molecular mechanisms underlying their activation and modulation are not fully understood[1–3]. Genetic studies have demonstrated critical roles for aGPCRs in development, immunity, and neurobiology, including brain development[4–8], myelination[9], brain angiogenesis[10], and neural tube development[11,12]. They are also linked to various diseases such as neurodevelopmental disorders, deafness, male infertility, attention deficit-hyperactivity disorder, schizophrenia, immune disorders, and cancers[6,13–16]. While 35% of FDA-approved drugs target GPCRs[17], aGPCRs have yet to be targeted therapeutically, primarily due to our limited understanding of their functional modulation.

The distinctive chimeric architecture of aGPCRs differentiates them from conventional GPCRs[13,18]. In addition to their signaling seven-transmembrane (7TM) helices that are characteristic of all GPCRs, aGPCRs also have large (up to 6000 residues), multidomain extracellular regions (ECRs). The ECR is characterized by a conserved GPCR Autoproteolysis INducing (GAIN) domain that is always positioned at the far C-terminus of the ECR, in close proximity to the 7TM region[19]. The GAIN domain contains an autoproteolysis site between its last two β-strands, and it is cleaved during protein maturation in the endoplasmic reticulum[19–21]. After autoproteolysis, the cleaved fragments stay non-covalently connected on the cell surface. The multidomain structure of the ECR allows it to interact with protein ligands found on adjacent cells or within the

[1]Department of Biochemistry and Molecular Biology, The University of Chicago, Chicago, IL, USA. [2]Neuroscience Institute, The University of Chicago, Chicago, IL, USA. [3]Institute for Biophysical Dynamics, University of Chicago, Chicago, IL, USA. [4]Center for Mechanical Excitability, University of Chicago, Chicago, IL, USA. [5]Department of Molecular Biosciences, Northwestern University, Evanston, IL, USA. [6]Present address: Department of Structural Biology, Genentech, South San Francisco, CA, USA. [7]These authors contributed equally: Szymon P. Kordon, Kristina Cechova. ✉e-mail: reza.vafabakhsh@northwestern.edu; arac@uchicago.edu

extracellular matrix. These interactions give rise to mechanical forces that are key for regulating receptor activation by modulating the accessibility of the last β-strand of the GAIN domain, that is also called the tethered agonist (TA) or Stachel peptide. Under normal conditions, the TA peptide lies within the core of the GAIN domain[22,23], but upon force-induced dissociation of the cleavage fragments, the TA peptide becomes exposed and can bind to the orthosteric site of the 7TM domain to activate the receptor[24–26]. Hence, according to the TA-mediated model of aGPCR activation, the ECR acts as a protective cap for the TA peptide to hide it within the GAIN domain.

Several recent observations suggest that other mechanisms of aGPCR activation are possible[27,28]. For example, some aGPCRs do not undergo autoproteolysis, which is required for TA release[29]. Even the aGPCRs that are cleaved do not always require cleavage for mediating some aspects of wild-type functions[7,29–31]. Specifically, functional data suggest that some aGPCRs are modulated by direct communication of the ECR with the 7TM[7,28,32–34]. Alterations to the ECR of aGPCRs, including alternative splicing, mutagenesis, or binding of synthetic proteins, have been shown to modify receptor signaling[32,35,36]. Furthermore, the removal of the ECR in ADGRG1/GPR56 increased the basal activity of the receptor[37]. Additionally, the TA mechanism implies that the receptor is used only once, which would be energetically costly for the cell, and does not provide a mechanism for how the signal can be turned off when the activating ligand dissociates from the ECR. Finally, compression forces that "push" on the receptor, for example, when cells are approaching each other during synapse formation, organogenesis or embryogenesis, might not be able to use the TA-mediated mechanism to activate the aGPCR. It has been suggested that the TA can regulate receptor signaling without coming out of the GAIN domain or by being partially exposed[38], however, the recent TA-bound 7TM structures of multiple aGPCRs showed that the critical phenylalanine residue and other important TA residues have to reach deep into the 7TM orthosteric pocket for receptor activation, suggesting that non-release or partial release of the TA is unlikely to activate the receptor[39–42]. Thus, accumulating data in the aGPCR field are consistent with an additional model in which the ECR conformation has a direct role in modulating the 7TM signaling, independently of TA-mediated activation[27,28,37,43].

In this ECR-mediated model for aGPCR activation, the ECR directly communicates with the 7TM (i.e. via transient interactions), such that ligand binding events or conformational changes in the ECR may directly result in altered signaling[27,28]. Direct proof of this model requires studying a holoreceptor, which is technically challenging. Several studies have determined the high-resolution structures of the isolated GAIN domain, other extracellular domains, and the 7TM from multiple aGPCRs[19,28,32,39–42,44–46]. However, none of these studies addressed how the extracellular region transduces the incoming adhesion signal to the membrane anchored 7TM domain as none of them could visualize the ECR and the 7TM simultaneously, leading to the assumption that the ECR might be flexible and not communicate with the 7TM directly. A full-length aGPCR structure, even at low resolution, is still missing, and characterization of the conformational dynamics of a full-length aGPCR remains absent.

ADGRL3, also known as Latrophilin3, is a prototypic aGPCR composed of lectin, olfactomedin, hormone binding (HormR), GAIN, and 7TM domains (Fig. 1a)[47]. Previous work has shown that ADGRL3 couples to Gα_s, Gα_{12/13}, Gα_i, and Gα_q[7,48–50]. ADGRL3 is highly expressed in the brain, where it is required for the establishment of excitatory synapses and for determining their specificity; and has been implicated in attention deficit-hyperactivity disorder and various cancers[7,15,51,52]. ADGRL3 mediates its synapse-formation function by its extracellular adhesive interactions with ligands, and, also, by its intracellular GPCR signaling[7,50,53–55].

Here, we used a combination of single-particle cryogenic electron microscopy (cryo-EM), single-molecule Förster Resonance Energy Transfer (smFRET), protein engineering, and GPCR signaling studies to map the relative orientation and conformational dynamics between the GAIN and 7TM domains of the ADGRL3 holoreceptor. We present that the holoreceptor has few, defined and slow-exchanging conformations in which the GAIN has restricted movement with respect to the 7TM as presented in the cryo-EM analysis and smFRET sensor Y795UAA on GAIN and sensors R933UAA, E1099UAA, and A871UAA on 7TM. The smFRET results confirmed the GAIN-7TM orientation revealed by the cryo-EM model. Further analysis showed that point mutations at the GAIN-7TM interface or GAIN-targeted antibodies that alter the downstream receptor signaling, also change the conformational distribution of GAIN in ADGRL3, demonstrating a direct link between receptor activity and the orientation of the GAIN domain with respect to the tip of TM1 and extracellular loops (ECLs) 1 and 3 of 7TM domain. Our results provide a structural and mechanistic understanding in support of the ECR-mediated activation of aGPCRs.

Results

Purification of ECR-bound ADGRL3 and development of synthetic antibody binders targeting the GAIN domain of ADGRL3

For structure determination, we recombinantly expressed human ADGRL3 containing HormR, GAIN, and 7TM domains (Fig. 1b) in *Spodoptera frugiperda* Sf9 cells, solubilized from membranes using n-Decyl-beta-Maltoside (DM), and purified by affinity chromatography using FLAG-tag. DM-solubilized ADGRL3 was then subjected to size-exclusion chromatography (SEC) with simultaneous detergent exchange to lauryl maltose neopentyl glycol (LMNG)/glyco-diosgenin (GDN) (Supplementary Fig. 1a). The sample quality was further confirmed by negative-stain electron microscopy (nsEM), that showed the uniform distribution of homogenous particles of the expected shape and size (Supplementary Fig. 1b–d). We previously reported that this construct is active in a G protein coupling assay[24], and further tested its activity using a serum response element (SRE)-luciferase assay that is commonly used as a likely readout for Gα_{12/13} signaling[24,35,48,56] and showed that it is active and has similar basal signaling as the full-length ADGRL3 (Supplementary Fig. 1e).

To aid the cryo-EM structural analysis of ADGRL3, we screened a synthetic antibody binder (sAB) library to obtain binders specific to the HormR/GAIN domains of ADGRL3. A biotinylated fragment of the ADGLR3 ECR containing HormR and GAIN domains was used as input for the generation of high-affinity sABs against ADGRL3 by phage display selection using a diverse synthetic phage library based on a humanized antibody Fab scaffold[57–59], and four rounds of selection were performed as described previously[35]. Following the selection and initial validation, we identified 10 unique HormR/GAIN binders by a single-point phage enzyme-linked immunosorbent assay (ELISA) (Supplementary Fig. 2a). Selected phagemids were then cloned into sAB protein format, expressed, and purified for further characterization. Two of the best-expressing sABs, named LK1 and LK3 bind to the ADGRL3 with low nanomolar affinity (3.3 and 3.9 nM respectively, Supplementary Fig. 2b), and form stable complexes with the receptor on SEC (Supplementary Fig. 2c, d) were chosen for structural and functional studies of ADGRL3.

Cryo-EM model of ECR-bound ADGRL3 reveals the orientation of the GAIN domain with respect to the 7TM region

For structure determination of ADGRL3, we used a neutral binder, LK3, that does not change the activity of the receptor in our SRE signaling assay (Supplementary Fig. 2e), and purified the ECR-bound ADGRL3 in complex with the sAB LK3 in LMNG/GDN detergent mix (Supplementary Fig. 2c). Addition of LK3 as a fiducial marker allowed for improved ADGRL3 2D classification and alignment, and enabled to obtain the overall cryo-EM projections of the complex in the micelle (Fig. 1c and Supplementary Fig. 3a). The conformational heterogeneity caused by the flexibility between the ECR and the 7TM domain restricted our
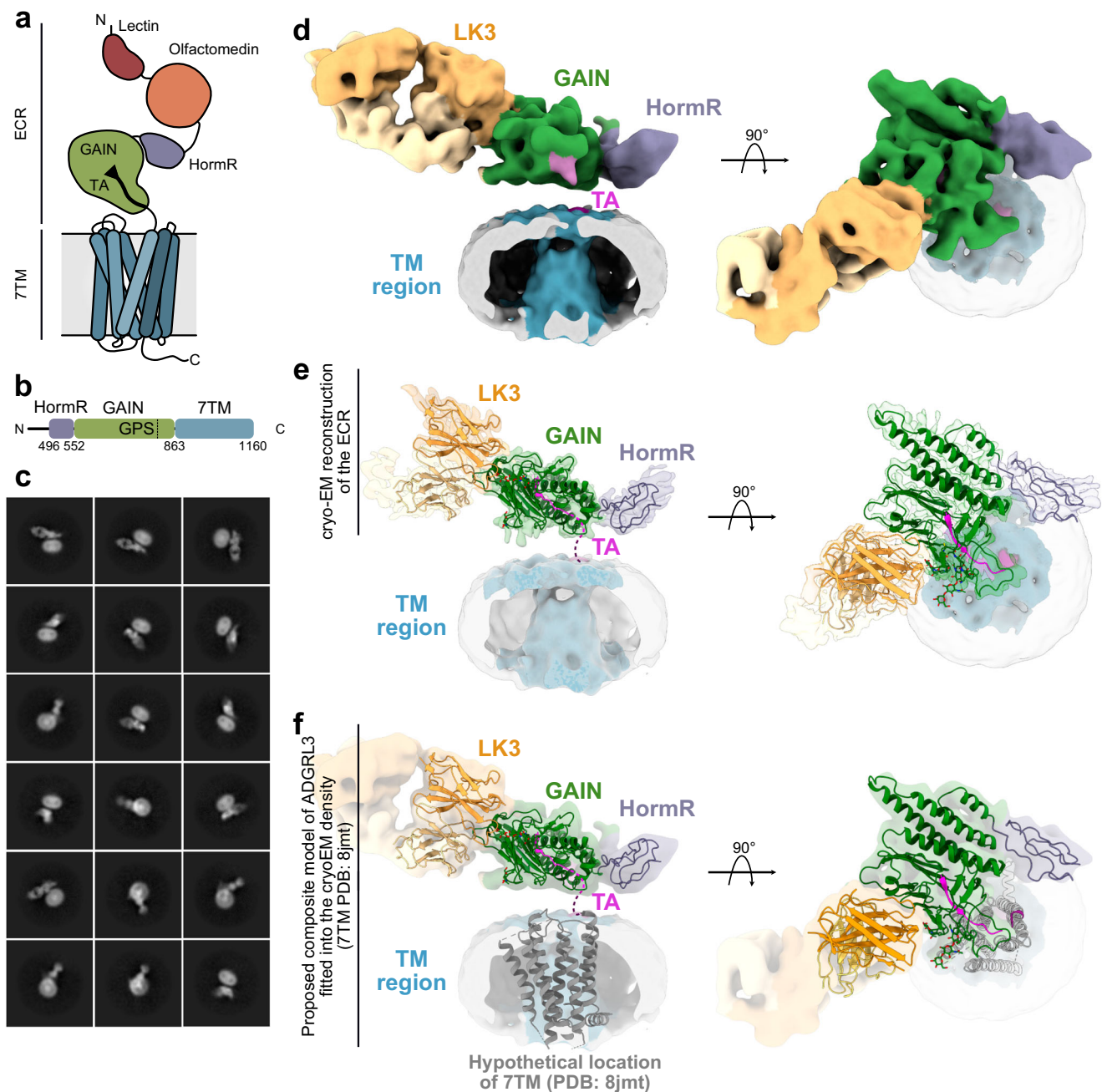
Fig. 1 | Cryo-EM model of ADGRL3/LK3 complex reveals the general architecture of the receptor and relative position of the GAIN domain in relation to the transmembrane region. a Cartoon representation of ADGRL3. The lectin domain is colored red, olfactomedin - orange, HormR - purple, GAIN - green, and 7TM in blue. The tethered agonist (TA) is presented as a black arrow within the GAIN domain. **b** Schematic diagram of domain boundaries of the ADGRL3 construct used for structural analysis. Domains colored as in (a). GPS represents GPCR Proteolysis Site. **c** Representative cryo-EM reference-free 2D class averages of the ADGRL3/LK3 complex purified in detergent micelle. **d** 6 Å low-pass filtered 3D map of ADGRL3 in complex with sAB LK3 at the threshold level set to 0.0375. Regions of the map corresponding to respective domains of the receptor and sAB are colored accordingly and labeled with domain names. The tethered agonist (TA) is colored magenta. **e** The composite map of ADGRL3 architecture consisting of a 3.9 Å structure of the HormR/GAIN domain in complex with sAB LK3, and a 6 Å low-pass filtered density for the micelle. **f** Proposed composite model of ADGRL3 holoreceptor. The hypothetical location of 7TM (available structure of apo-state ADGRL3 corresponding to PDB: 8jmt) is placed in the membrane region.

attempts to obtain a high-resolution structure of the entire ADGRL3 molecule. In contrast to previous studies on ADGRL3, we did not utilize the addition of G proteins to lock the 7TM region in an active state[39,49]. As a result, the ECR with sAB bound being a more distinctive feature dominated the alignment, causing the density for the transmembrane region to be washed out during 3D averaging, and absent in the final map of the ADGRL3 (Supplementary Fig. 3b). The nominal resolution of the entire complex model was 5.5 Å, with most of the ECR resolved to 4 Å, and micelle region limited to ~10 Å (Supplementary Figs. 3a–c, 4a, Supplementary Movie 1, and Supplementary Table 1). However, given the current quality of the map, we can define the position of the GAIN domain in relation to the detergent micelle (Fig. 1d, e). The overall architecture of the receptor suggests that the GAIN domain of ADGRL3 lays flat, with a parallel orientation in relation to the membrane, and does not adapt the extended, vertical position as suggested by AlphaFold2 structure predictions[60] (Supplementary Fig. 5). Even
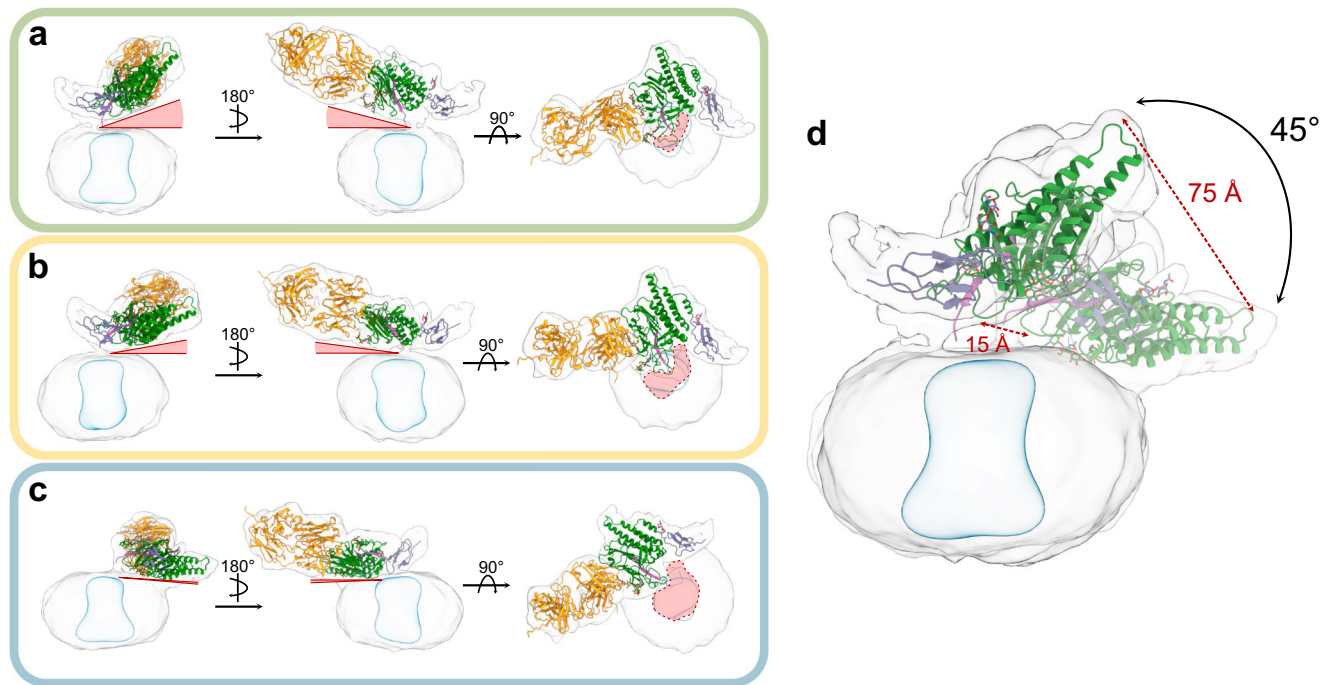
Fig. 2 | Cryo-EM 3D variability analysis presents constrained flexibility of the ADGRL3 GAIN domain. a–c Side and top views of representative low-resolution 3D models from 3D variability analysis show the degree of HormR/GAIN domain movement in relation to the detergent micelle. Models from **a** the first frame of 3D variability analysis, showing the most vertical orientation of the GAIN domain seen within the dataset; **b** The middle frame of 3D variability analysis, presenting the intermediate position of the GAIN domain; **c** The last frame of 3D variability analysis, showing the most horizontal orientation of the GAIN domain. The red triangles on each panel depict the degree of the angle between the bottom of the GAIN domain and the plane of the micelle. The red areas highlighted on the top-view projections show the increasing access of the transmembrane region to the extracellular space with the GAIN domain pulling away from the central axis. **d** Superimposition of the most distinct frames (**a**, **b**) showing the distances and angle between two GAIN conformations. Structures of HormR/GAIN domains of ADGRL3 in complex with LK3 are placed in the maps by rigid body fitting.

though the transmembrane domain was not resolved, a 6 Å low-pass filtered map of the ADGRL3 presented a vertical density in the middle of the detergent micelle that could accommodate the transmembrane region of the receptor (Fig. 1d, e and Supplementary Movie 1). This allowed us to propose the hypothetical composite model of ADGRL3, by placing the TM1 of the available structure of apo-state ADGRL3 7TM (PDB: 8jmt[46]) in close vicinity to the linker connecting it to the GAIN domain. The covalent connection between the C-terminus of the GAIN domain and the N-terminus of the TM1 acted as an anchor point for placing the 7TM structure into the hypothetical model (Fig. 1f). Though at our current reconstruction quality, we are unable to describe any potential interaction between GAIN and 7TM regions, GAIN stays in close proximity to the 7TM within the membrane. These results show that, unlike previous assumptions, the GAIN and 7TM domains are not fully flexible, and the GAIN domain has a defined orientation with respect to the 7TM domain.

To better understand the extent of the ECR/7TM flexibility in the ADGRL3 model, we performed a 3D Variability analysis and found that the ECR can sample several other conformations within a restricted space over the membrane (Fig. 2a–c and Supplementary Movie 2)[61]. Despite this, the scope of the ECR movement retains the overall orientation of the GAIN domain, with the same side of the GAIN always facing the membrane. Comparing all conformations to the consensus model, the GAIN domain can either adopt a more upright conformation, staying right above the detergent micelle (Fig. 2a), or lay closer to the membrane surface, shifting laterally away from the center of the micelle (Fig. 2c). However, the movement of the GAIN domain is constrained to a small volume, and does not sample the full extent of the available volume (calculated approximately to 30% of the total possible volume it may occupy). The magnitude of the GAIN movement between the two most distant conformations is around 45° and varies

between 15 Å distance change close to the membrane (and hypothetical 7TM orientation) and 75 Å change at the tip of the GAIN domain (Fig. 2d).

3.9 Å structure of HormR/GAIN domains reveals a fully hidden TA within the GAIN domain

Utilizing local refinement, we determined the 3.9 Å structure of ADGRL3 HormR/GAIN domains bound to LK3 within the context of the holoreceptor[62] (Figs. 1e, 3a and Supplementary Table 1). The structure shows the conserved HormR/GAIN fold, with the N-terminal subdomain A of the GAIN domain composed of six α-helices and the C-terminal subdomain B including 13 β-strands, as previously reported in crystal structures of isolated HormR/GAIN domains (Supplementary Fig. 6)[19,45]. Importantly, we observed a distinct density that corresponds to the TA peptide in holo-ADGRL3. The TA peptide, including residues crucial for TA-dependent activation (specifically F857, L860, and M861), remains buried within the GAIN domain. The TA peptide is inaccessible to the solvent and positioned away from the orthosteric pocket within the 7TM domain, despite the flexibility of the ECR (Fig. 3b). All well-resolved residues of the TA peptide (T855-E865) form a strong network of hydrogen bonding, and numerous hydrophobic interactions, with total interface area of 1100 Å^2, similar to that of isolated GAIN domains. Additionally, there is no evidence of the TA peptide coming out of, or getting partially exposed from the GAIN domain or interacting with the 7TM domain. These results are inconsistent with a partial TA-exposure-mediated activation mechanism and favor a direct ECR-mediated activation mechanism.

Furthermore, we observed densities at N-linked glycosylation sites on residues N843 and N817 that are conserved within ADGRLs (Fig. 3c, d). Specifically, the low-threshold map of the GAIN domain showed a density for a long glycan moiety attached at position 843,
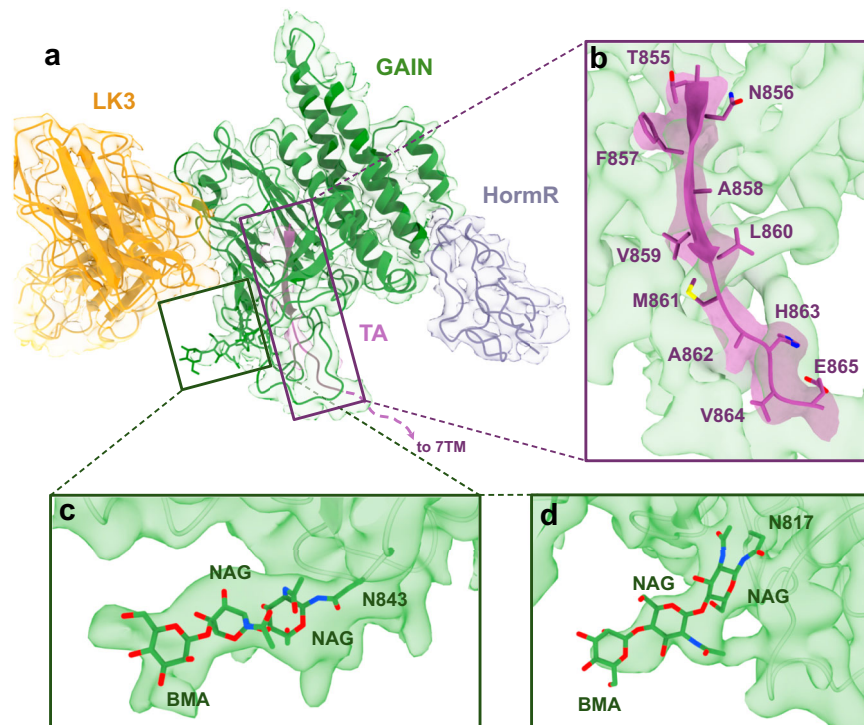
Fig. 3 | Cryo-EM structure of the 7TM-bound ADGRL3 HormR/GAIN domains at 3.9 Å resolution. a The cryo-EM structure and density map of HormR/GAIN domains of ADGRL3 bound to sAB LK3. HormR domain is colored purple, GAIN - green, TA - magenta, and heavy and light chains of LK3 - yellow. **b** Close-up view of the intact TA buried within the GAIN domain in the holoreceptor. Side chains of the TA peptide are shown as sticks. **c** and **d** Glycosylation of conserved sites N843 (**c**) and N814 (**d**) at the membrane-facing side of the GAIN domain modeled into the density map of HormR/GAIN domains.

running alongside the bottom face of the GAIN domain, parallel to the membrane. It is possible that this long sugar addition may be important for maintaining the GAIN domain conformation and the orientation of the entire ECR with respect to the 7TM and the membrane, as in the case of EGFR[63] and thyrotropin receptor ectodomains[64]. It has been shown that electrostatic interactions accompanied by steric effects between glycan chains in the protein and the membrane surface can be critical for the arrangement of extracellular domains[65].

The cryo-EM structure also allowed us to elucidate the molecular basis of the interaction between LK3 and ADGRL3 ECR. LK3 binds to the side of the GAIN domain through CDRs in both heavy (H1, H2, and H3) and light chains (L3), resulting in a total interface area of 835 Å^2 in the complex (Supplementary Fig. 7). This interface is mediated mainly by bulky, aromatic residues of LK3 CDRs and involves extensive hydrogen bonding and van der Waals interactions with residues in subdomain B of the GAIN domain. Notably, hydrogen bonds between Y36$_{H1}$ and A797$_{ADGRL3}$/D798$_{ADGRL3}$, S58$_{H2}$ and L796$_{ADGRL3}$/A797$_{ADGRL3}$, Y104$_{H3}$ and L796$_{ADGRL3}$, W105$_{H3}$ and S850$_{ADGRL3}$, W108$_{H3}$ and P799$_{ADGRL3}$, Y112$_{H3}$ and D798$_{ADGRL3}$/N730$_{ADGRL3}$, Y95$_{L3}$, and N730$_{ADGRL3}$, stabilize the interaction and shape the total buried surface area (Supplementary Fig. 7).

Real-time measurement of conformational changes via smFRET present three stable conformations for GAIN/7TM

To map the conformational landscape of the full-length ADGRL3 and directly visualize the relative orientation and dynamics of the GAIN domain with respect to the 7TM domain, we used single-molecule Förster resonance energy transfer (smFRET). We used restraints from our cryo-EM reconstruction to design multiple smFRET sensors that will test the validity of the relative orientation of the GAIN domain with respect to the 7TM. To minimize perturbations to the receptor structure we used unnatural amino acid incorporation and click chemistry for site-specific labeling of the receptors[66,67]. With this approach, we

generated multiple FRET sensors to probe the relative orientation of the GAIN and the 7TM domains. Specifically, we focused on three FRET sensors with fluorophores between positions Y795UAA (within the loop in the subdomain B of the GAIN) and R933UAA (within ECL1), E1099UAA (within ECL3), and A871UAA (on tip of the TM1) (Fig. 4a). Receptors harboring the unnatural amino acids were expressed in HEK293T cells and site-specifically labeled with FRET donor (Cy3) and acceptor (Cy5) fluorophores and showed strong labeling on the plasma membrane (Fig. 4b). After solubilization with the detergent, receptors were applied onto a polyethylene glycol (PEG)-passivated coverslips with an anti-GFP-tag antibody for total internal reflection fluorescence (TIRF) imaging[68] (Fig. 4c).

We found that in the absence of any ligands or external stimuli, the GAIN domain was dynamic, as shown from the three sensors (Fig. 4d and Supplementary Fig. 8). This is consistent with the overall conclusion from our cryo-EM analysis. Interestingly, we found that the GAIN domain undergoes a transition between defined conformational states with respect to the 7TM domain rather than a continuum of states. Importantly, quantitative analysis revealed that in each of the three sensors transition happened between up to three distinct conformations of the GAIN domain with respect to the 7TM domain (Fig. 4d–f). For the Y795:A871 sensor, we found that 44% of traces showed a single FRET state, 48% showed two FRET states, and 8% showed three FRET states before photobleaching (Supplementary Fig. 9). For this sensor, the three FRET states that were consistently visited were 0.44, 0.55, and 0.65 (Fig. 4e, f). This is in qualitative agreement with the approximate distances between these residues in the GAIN/7TM models that were fit into the three cryo-EM conformations, which are ~61, ~57, and ~54 Å (measured from the α-carbon). Our findings reveal that the GAIN domain undergoes transitions between distinct, discrete conformational states relative to the 7TM domain, offering crucial insights into the receptor's constrained structural flexibility and is in general agreement with the cryo-EM analysis.
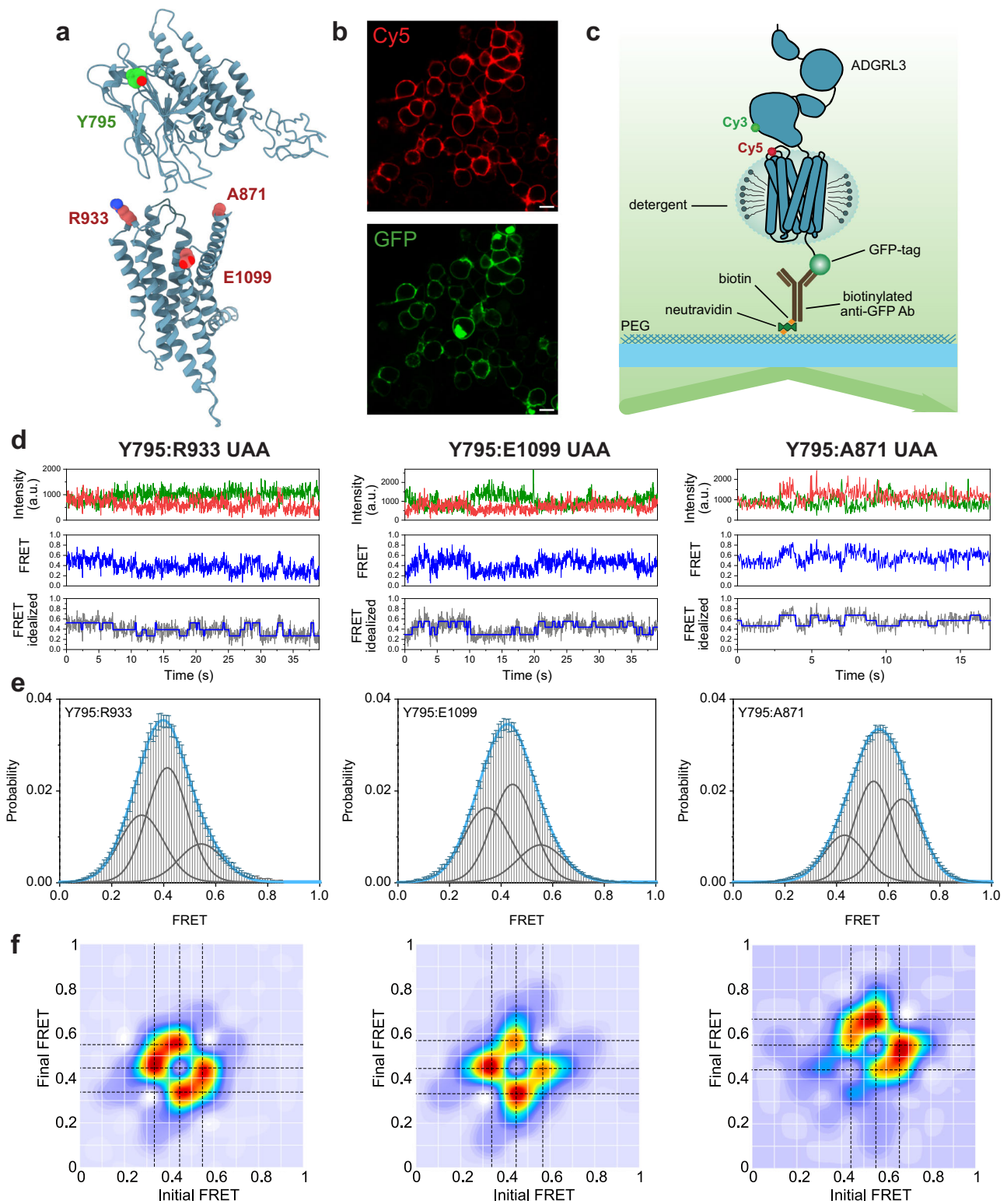
Fig. 4 | smFRET present three stable conformations of ADGRL3 ECR/7TM.
a Hypothetical model of ADGRL3 (containing HormR, GAIN, and 7TM domains) showing positions of amino acids that were replaced by UAA in making of the smFRET sensor pairs: Y795 (in green), R933, E1099, A871 (in red). **b** Example of confocal microscopy images of ADGRL3-UAA labeled with Cy5 (red) showing membrane expression and GFP (green) showing overall expression of the receptor. Images are representative samples of $n = 3$, independent biological replicates. Scale bar: 10 μm. **c** Schematic of SiMPull smFRET TIRF microscopy experiment. **d** Representative smFRET traces of Y795:R933 UAA, Y795:E1099 UAA, and Y795:A871 UAA, showing donor (green) and acceptor (red) intensities, corresponding FRET (blue), and idealized FRET trace (blue line over gray FRET data)

from HMM. **e** Single-molecule FRET population histograms of Y795:R933 UAA, Y795:E1099 UAA, Y795:A871 UAA, respectively (error bars represent s.e.m., $n = 3$, independent biological replicates). Three single Gaussian distributions (gray) were fitted to the histograms. Peaks are centered at 0.32, 0.41, and 0.54 for Y795:R933 UAA, 0.35, 0.44, and 0.55 for Y795:E1099 UAA, and 0.45, 0.55, 0.65 for Y795:A871 UAA. The cumulative fit is overlaid in blue. Source data are provided as a Source Data file. **f** Transition density plots of Y795:R933 UAA, Y795:E1099 UAA, and Y795:A871 UAA, respectively ($n = 3$, independent biological replicates). Dashed black lines cross the most observed transitions between different states and were considered in the multiple-peak fitting of smFRET histograms.

Synthetic antibodies can activate ADGRL3 and alter the conformational distribution of GAIN/7TM

The binding of synthetic ligands to the ECR of ADGRL3 and other aGPCRs can alter receptor signaling[28,35,36,69,70]. We tested the effect of sABs LK3 and LK1 binding on ADGRL3 signaling activity using the SRE-luciferase assay[24]. LK3, which was used for cryo-EM studies, did not change the basal activity of the receptor when compared to the control experiment, acting as a neutral synthetic binder for ADGRL3 in the SRE assay (Supplementary Fig. 2e and Fig. 5a). On the other hand, addition of LK1 resulted in a substantial increase in signaling compared to untreated sample or LK3 (Fig. 5a).

Next, we wondered whether sABs that affect ADGRL3 downstream signaling would alter the ECR-to-7TM orientation. We speculated that if the antibodies alter receptor signaling purely via the TA-activation model, the ECR-7TM orientation would be independent of receptor signaling; whereas if the antibodies alter receptor signaling via the ECR-mediated mechanism, receptor signaling would depend on the ECR/7TM orientation. To test this, we performed similar smFRET measurements with the sensor Y795UAA:A871 UAA in the presence of LK1–as the activating sAB, and LK3–as the neutral binder. Both in the presence of 1 μM LK1 and 1 μM LK3, the ECR still remained dynamic while transitioning between the same three states as the apo receptor (Fig. 5b-e). While the percentage of traces showing one, two, or three FRET states before photobleaching were the same with LK1 compared to the apo receptor (Fig. 5f), we found that the overall FRET histogram shifted toward lower FRET (Fig. 5g), increasing occupancy of the lowest FRET peak at 0.44 by 18% while decreasing the occupancy of the FRET states at 0.55 and 0.65 by about 9% in each case (Fig. 5h). Consistently, among the traces that were stable in a single FRET state before photobleaching, the percentage of traces that were in FRET 0.44 increased by 22%, but decreased for the higher FRET states (Fig. 5i). Together these results support the notion that the agonist LK1 increases the stability of the lowest FRET state. Therefore, the lowest FRET state of 0.44 is likely associated with higher receptor activity as assessed by the SRE assay.

Unlike LK1, neutral binder LK3 did not change the occupancy of the FRET states compared to the apo receptor (Fig. 5g-i). Finally, control experiments with a nonspecific sAB showed no change in FRET histogram (Supplementary Fig. 10). We also performed dwell time analysis for traces from the WT receptor in the absence or presence of LK1 or LK3 (Supplementary Fig. 11). We found that addition of LK1 increases the dwell time of FRET state at 0.44 by 77% while reducing the dwell time of the FRET state at 0.65 by 36%. Importantly we did not observe a significant change in the dwell time of FRET states in the presence of LK3, as expected from a neutral binder (Supplementary Fig. 11). Taken together, these results suggest that different conformations of the ECR have different signaling capacities and specific antibodies can modulate the conformational distribution of the ECR to modulate the SRE signaling output without locking the ECR into a specific conformation.

We then used cryo-EM single particle analysis to visually observe the effect of LK1 on the ECR orientation in relation to the detergent micelle and the hypothetical 7TM position of ADGRL3. The low-resolution cryo-EM map showed that LK1 binds to a different epitope on the GAIN domain when compared to the LK3-bound model (Fig. 5j, Supplementary Fig. 12, and Supplementary Table 1). LK1 positions itself on top of the GAIN domain, possibly pushing it down. This causes the GAIN domain to bend closer to the membrane, while moving sideways away from the central axis of the 7TM region. This orientation of the GAIN domain suggests that LK1 might activate the receptor by pushing/pulling forces extorted to the ECR.

Cancer-associated mutations at the GAIN/7TM interface shift ECR/7TM conformation

To further explore and confirm the relationship between the ECR conformation and receptor function, we performed experiments with previously described cancer-associated mutations S810L/E811Q. These residues are positioned on one of the exposed loops of the GAIN domain that faces the 7TM in our cryo-EM model (Fig. 6a)[19,71]. Recent work showed that ADGRL3 signaling through $G\alpha_{12/13}$ was impaired by the single-point cancer-related mutations S810L and E811Q[71] although the mutations had no effect on autoproteolysis and are not a part of the TA[19]. These observations suggested that the GAIN domain could make transient interactions with the extracellular loops on the 7TM.

Interestingly, we found that in the presence of the S810L/E811Q mutation, the smFRET distribution shifted towards higher FRET values compared to the WT receptor (Fig. 6b, c). Quantification of FRET traces showed that there was no significant difference in the overall distribution of the number of states per individual trace between the WT and mutant receptor (Fig. 6d). However, the occupancy of high FRET state at 0.65 was significantly increased from 32 to 56% for the S810L/E811Q mutant compared to the WT receptor and the occupancy of other FRET states at 0.44 and 0.55 decreased (Fig. 6e). Consistent with this, among the traces that showed a single FRET state during the recording, the fraction of traces at FRET 0.65 increased from 16 to 58%, almost entirely at the expense of reduction in traces at 0.44 (Fig. 6f). Finally, we found that addition of 1 μM LK1 to this mutant receptor shifted the FRET histogram towards to the lower FRET values and similar to the WT receptor (Fig. 6g) by reducing the occupancy of the highest FRET state at 0.65 and increasing the occupancy of the lowest FRET state at 0.44 (Fig. 6h, i). Importantly, the addition of the neutral binder LK3 to this construct did not change the smFRET distribution or occupancy of each of the states compared to the WT (Supplementary Fig. 13). Together, these results are consistent with the notion that the highest FRET state at 0.65 for this sensor corresponds to lower $G\alpha_{12/13}$ signaling propensity.

Discussion

In this work, we aimed to elucidate the structural features and conformational dynamics of ECR-bound aGPCRs to better understand the molecular nature of the crosstalk between the ECR and 7TM regions of aGPCRs. aGPCRs are cell-surface receptors that have key roles in a vast variety of physiological functions that range from embryogenesis to immunology, and neurobiology to organogenesis. aGPCR have multidomain ECRs that participate in cell-cell adhesion, communication, and signal transduction[13,18,72]. Despite the recent emergence of structural and functional data, the conformational landscape between the ECR and 7TM regions in a holoreceptor is uncharacterized, and how exactly aGPCRs convert ECR-mediated cellular adhesion into transmembrane signaling is not known. The TA-mediated activation mechanism of aGPCRs has been extensively studied, and structures of TA-bound transmembrane helices of aGPCRs have been determined[39–42,49]. However, multiple lines of evidence from different labs suggest that the TA-mediated mechanism may not be the only one underlying many physiological functions of aGPCRs. The cleaved TA is tightly locked in a conserved hydrophobic pocket within the GAIN domain and is surrounded by 15 backbone hydrogen bonds observed in all known GAIN domain structures, making its release chemically and physically difficult. Based on GAIN domain structures, the force that is required to expose the TA has been reported to be as high as 200 pN[73,74], raising the question of whether all aGPCRs detect such high physical forces on the receptor in a cellular environment. These results imply that most aGPCRs are insensitive to forces in the range of 2–40 pN where most receptor-ligand mediated biological forces
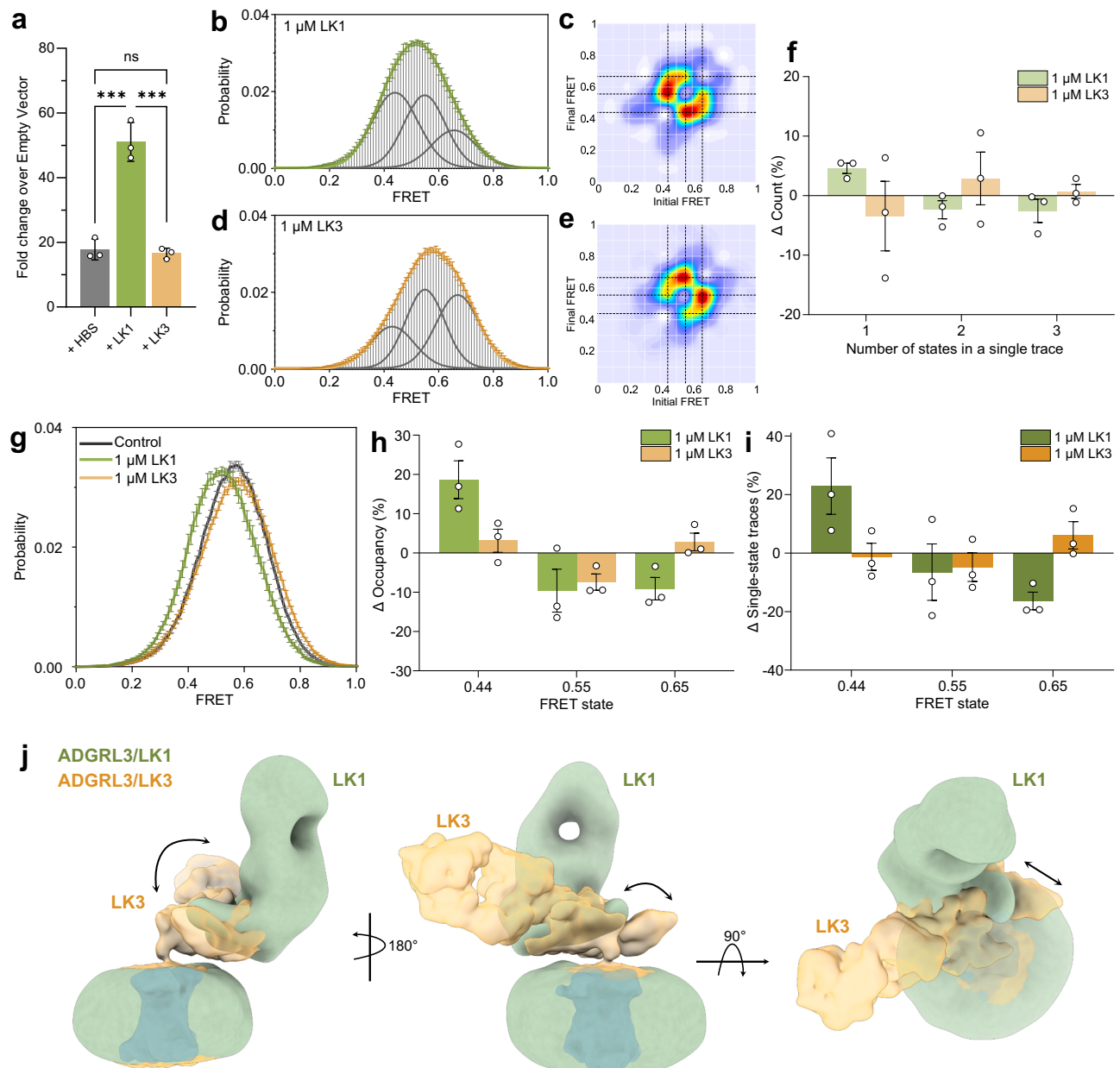
Fig. 5 | Binding of the activating sAB LK1 increases the occupancy of the lowest FRET peak. a SRE-luciferase assay for signaling of ADGRL3 in the presence of 1 μM purified sABs LK1 and LK3 presented as fold increase over empty vector. Data were presented as mean ± SD of three repeats (*n* = 3) for a representative of three independent experiments. ***p = 0.0001; vs. HBS buffer treatment; two-way ANOVA. **b** smFRET population histogram of Y795:A871 UAA sensor in the presence of 1 μM LK1 antibody. Three single Gaussian distributions (gray) were fitted to the histogram centered at 0.44, 0.55, and 0.65 with cumulative fit in green. **c** Transition density plots of Y795:A871 UAA sensor with 1 μM LK1. Dashed lines indicate the most frequent transitions. **d** smFRET population histogram of Y795:A871 UAA sensor pair in the presence of 1 μM LK3 antibody. Three single Gaussian distributions (gray) were fitted to the histogram centered at 0.44, 0.55, and 0.65. The orange line represents the cumulative fit. **e** Transition density plots of Y795:A871

UAA sensor pair with 1 μM LK3. Dashed lines indicate the most frequent transitions. **f** Percent change in the number of states occurring in individual traces in the presence of antibodies LK1 or LK3 versus the apo receptor. **g** smFRET population histograms of Y795:A871 UAA sensor pair in control conditions in the presence of 1 μM LK1 or 1 μM LK3. **h** Change in occupancy of the three FRET states after the addition of LK1 or LK3 compared to the apo state. **i** Change in the occurrence of different FRET states among traces that showed only one state during recording between apo and LK1 or LK3 condition. **j** Superimposition of low-resolution maps of ADGRL3 in complex with sABs LK3 (in yellow) and LK1 (in green) showing a shift in the HormR/GAIN domains position in relation to the micelle. **b**–**i** Data represent mean ± s.e.m., *n* = 3 from three independent biological replicates. Source data for panels **a**, **b**, **d**, **f**, **g**, **h**, **i** are provided as a Source Data file.

fall[75–78] or to compression forces that push on the receptor, which may be common during synapse formation, organogenesis, and embryogenesis[79–81]. In addition, some aGPCRs such as ADGRLs and CELSRs function independent of autoproteolysis, which is a prerequisite for TA-dependent mechanism[7,29,31].

The GAIN domain has stable positions with respect to the 7TM domain
Here we report the overall architecture of the ECR-bound ADGRL3 and define the relative position of the GAIN domain to the membrane. Our cryo-EM data provided the high-resolution structure of the
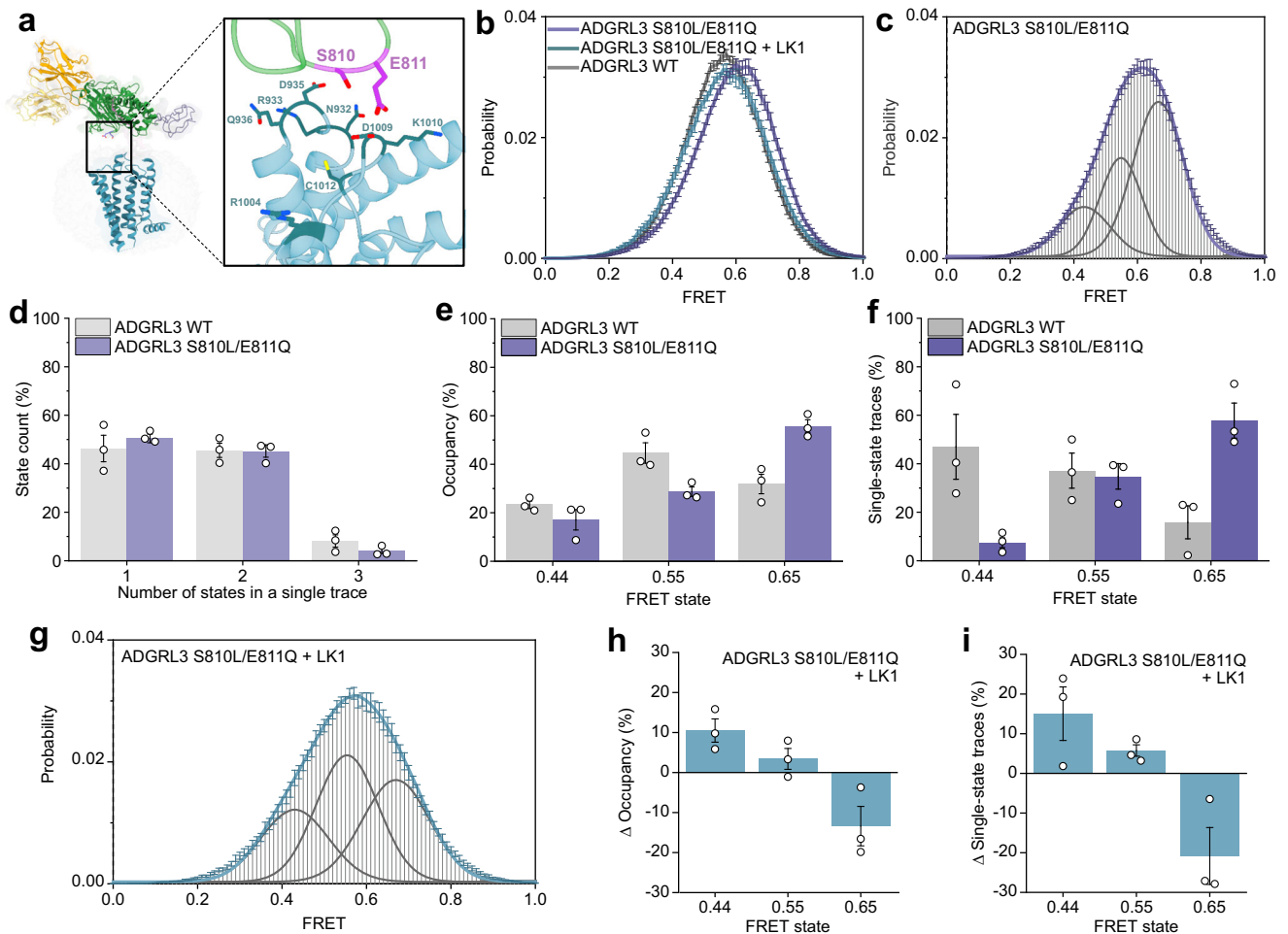
Fig. 6 | Cancer-associated GAIN domain mutant shifts the smFRET peaks to higher FRET. a Model of ADGRL3 showing positions of residues S810/E811 in purple, with potential interaction residues from extracellular loops of 7TM shown as sticks (blue). **b** Compilation of smFRET population histograms of ADGRL3 for the sensor Y795:A871 UAA and for mutant S810L/E811Q with or without 1 μM LK1 and ADGRL3 WT. **c** smFRET population histogram of ADGRL3 mutant S810L/E811Q fitted to three Gaussian distributions (gray) centered at 0.44, 0.55, and 0.65. The cumulative fit is purple. **d** Number of states (%) occurring in individual traces from WT ADGRL3 and S810L/E811Q mutant. **e** Occupancy of the three FRET states in WT and S810L/E811Q mutant ADGRL3. **f** Occurrence of the three individual FRET states (0.44, 0.55, and 0.65) among single-state traces. **g** smFRET population histogram of ADGRL3 mutant S810L/E811Q in a presence of 1 μM LK1 antibody. Histogram was fitted to three Gaussian distributions (gray) with centers at 0.44, 0.55, and 0.65. The blue line is the cumulative fit. **h** Change in the occupancy of the three FRET states after addition of 1 μM LK1 to ADGRL3 mutant S810L/E811Q **i** Change in the percentage of different FRET states among all traces that stayed in a single state throughout the recording in the presence of 1 μM LK1 compared to apo receptor. **b**–**i** Data represent mean ± s.e.m. (n = 3), of three independent biological replicates. Source data are provided as a Source Data file.

extracellular region with respect to the membrane, although it lacked a well-defined density for the transmembrane region. Despite the low resolution, our model reveals that the ECR is not completely flexible as previously assumed and has a preferred orientation with respect to the membrane. The smFRET sensors that were designed based on the cryo-EM model have helped us determine the relative position of the 7TM in relation to the GAIN domain. Based on these results and the presence of a covalent linker between the TA peptide and TM1, we proposed a hypothetical position of the transmembrane region. However, we cannot exclude other potential orientations of the transmembrane domain, particularly along the central vertical axis of the receptor. We found that the GAIN domain lays flat, in close proximity to the membrane, and does not display a large extent of flexibility, limited to a 45° range of movement. 3D variability tools showed that GAIN samples other conformations, all of which maintain the overall arrangement of the domains. Furthermore, smFRET experiments with full-length ADGRL3 show that the GAIN domain adopts three stable conformations with respect to residues R933 (ECL1), E1099 (ECL3), and A871 (TM1) on 7TM. These conformations

have slow exchange rates between each other and switch from one to another in an orderly manner. With these results, we propose that the GAIN/7TM of ADGRL3 displays restricted flexibility, with limited range of motion between the two regions of the receptor, and adopting distinct and stable conformations (Fig. 7). Though our interpretation seems contrary to previous studies that reported high flexibility of the ECR, it is possible that ECR stays more rigid in the basal state and becomes more flexible when the receptor is activated, as numerous such studies captured the active conformation of the 7TM complexed with trimeric G proteins.

Importantly, we have not observed the TA peptide dissociation from the GAIN domain or partial exposure to the 7TM domain, which would be consistent with the partial TA-exposure model. The high-resolution map of the GAIN domain from ECR-bound ADGRL3 includes the density of the intact TA peptide, suggesting that the TA peptide, especially the conserved F857, L860, and M861 residues, that dive deep into the 7TM domain to enable TA-mediated activation, are not exposed to the 7TM when the receptor is at its basal state. This observation is in favor of an ECR-mediated and TA-independent
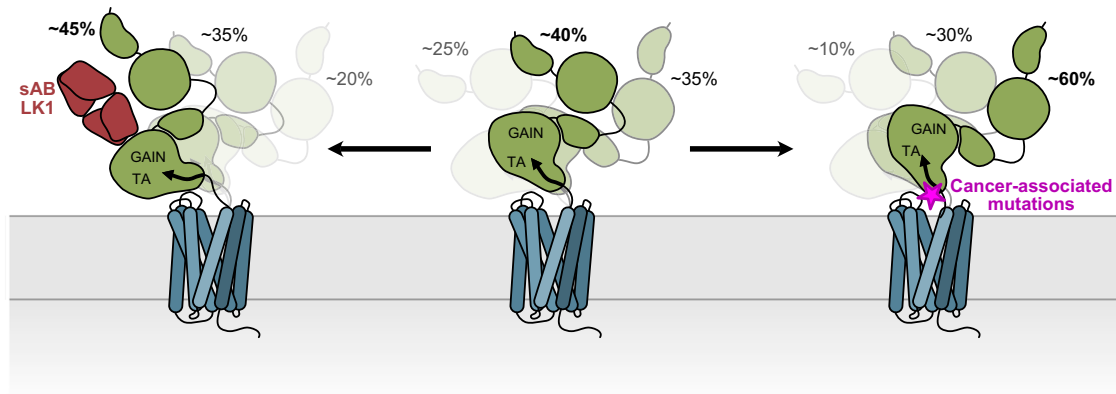
Fig. 7 | Antibodies and disease mutations at the ECR/7TM interface change the distributions of ADGRL3 holoreceptor conformations. Schematic cartoon of the effects of sAB LK1 and cancer-associated mutations on conformational dynamics of ECR in ADGRL3. Activating sAB LK1 stabilizes the lower FRET states, while cancer mutants stabilize the higher FRET states of ADGRL3.

mechanism of aGPCR activation, especially for aGPCRs that are not cleaved in the GAIN domain.

Interestingly, the orientation of the GAIN/HormR fragment in the model positions the HormR domain in close proximity to the membrane and 7TM region. This suggests that other more N-terminal domains of the ECR can potentially also remain closer to the membrane, forming a compact multidomain module[82], rather than freely sampling extracellular space in search of binding partners. The structures of isolated full ECR of both ADGRG6/GPR126[32] and ADGRC1/CELSR1[82] present compact conformations; similarly, an AlphaFold2 prediction of ADGRL3 full-length ECR places the Lec/Olf domains close on top of the extracellular facing surface of the GAIN domain, making a compact module (Supplementary Fig. 14). Furthermore, several functional studies have shown that deletion of N-terminal domains from different aGPCRs including ADGRG1/GPR56, ADGRG6 and ADGRL1 affected the basal activity of the receptors[24,32,34]. In addition, the same conclusion was achieved from the observations that the binding of antibodies or endogenous ligands to most N-terminal domains of aGPCRs also changed receptor signaling and function[28,35,36,69,70]. Put together, this suggests that the ECR of some aGPCRs may adopt a tightly packed conformation that transmits information from the N-terminal to C-terminal ECR domains, and to the 7TM.

Agonistic antibodies and disease mutations at the ECR/7TM interface change the ECR/7TM conformation

LK1 antibody which binds to the ECR and modulates receptor activity, also changes the distribution of the population of conformations in the smFRET assays, indicating a correlation between each ECR conformation and the signaling level of the receptor in the SRE assay (Fig. 7). This implies that the activation by the antibody does not require ECR dissociation as no dissociation was observed in smFRET traces. A low-resolution model of LK1 bound to ADGRL3 further confirms the intact LK1/ADGRL3 complex and presents a different orientation of the GAIN domain. Similarly, cancer-associated mutations that are shown to decrease the receptor activity in SRE assay also change the population of smFRET conformations, suggesting that a shift in the populations of conformations might underly reduction in receptor signaling[71] (Fig. 7). A local change in the transient interdomain interaction of the GAIN and 7TM domains likely induces small and tunable changes in receptor activity. Our data suggest that the highest FRET state corresponds to the lower receptor signaling, and the lowest FRET state corresponds to the higher basal receptor signaling. Thus, our results suggest that ECR conformation and dynamics correlate with downstream receptor signaling as measured by the SRE assay.

Because the SRE assay is commonly used as a likely readout for $G\alpha_{12/13}$ signaling, we also tested the effect of ECR perturbations using an additional assay, the cAMP assay that is used as a readout for $G\alpha_{s/i}$ signaling. Our observations hinted at signaling bias that is caused by ECR conformation. We observed that the ADGRL3 construct containing HormR/GAIN and 7TM had higher basal activity than the full-length ADGRL3 in the cAMP assay, unlike in the SRE assay (Supplementary Fig. 1e, f); and that both the LK3 and LK1 sABs acted as neutral binders in the cAMP assay although LK1 was an agonist in the SRE assay (Supplementary Fig. 2e, f). These observations suggested that while ECR conformation and dynamics affect downstream signaling, the effect is not identical in different signaling readouts. This idea was strengthened when we tested the N-linked glycosylation site mutations in the SRE and cAMP assays and observed no effect on the SRE assay and smFRET conformations, but observed an effect on the cAMP signaling (Supplementary Fig. 15). We hypothesize that the observed conformations of the holoreceptor can activate a certain signaling pathway while the same conformations are inactive for the other signaling pathways and vice versa. This potential signaling bias opens new directions for further studies on aGPCRs.

An ECR-mediated mechanism of aGPCR activation to sense pushing as well as pulling forces

Most importantly, our results provide evidence for the ECR-mediated activation of aGPCR as a complementary mechanism for the TA-mediated activation of aGPCRs. Many biological forces are smaller than 200 pN, the force that is needed to separate the TA from the GAIN domain[75-78]. To sense these smaller forces, to regulate aGPCR function on and off, and to activate uncleaved aGPCRs, a mechanism that does not depend on ECR dissociation and TA exposure might be at work. At low force or no force conditions, aGPCR may be reversibly regulated by binding and dissociation of a ligand to the ECR without ECR shedding and TA exposure (Fig. 8). In this model, the ECR-7TM communication is altered by transient interactions between ECR and 7TM. The TA peptide remains at its original position and is not involved in signaling. Because the TA-mediated mechanism is a "one and done" mechanism that is irreversible and prevents the receptor from going back to its inactive resting state, the ECR-mediated mechanism may operate in situations where a reversible regulation is needed. The ECR-mediated mechanism may also enable responding to compressing forces on the receptor, that directly "push" on the protein (Fig. 8). In cases where a large "pulling" force is executed on the ECR, the ECR may be removed from the 7TM releasing the tethered agonist and activating the aGPCR irreversibly but acutely (Fig. 8). Future work that dissects different activation mechanisms of aGPCRs in different
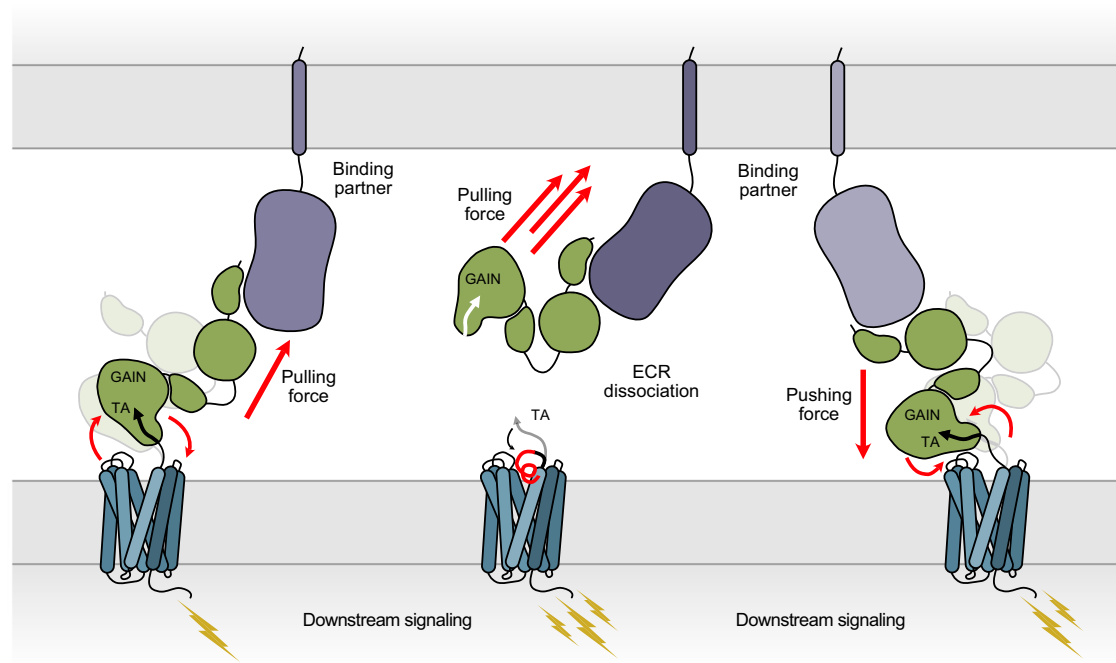
Fig. 8 | Proposed ECR-mediated activation mechanisms of adhesion GPCRs. Binding of an extracellular protein ligands subject aGPCR to a range of potential forces. A small pulling force can activate the holoreceptor by changing the conformation of the ECR and inducing the signal transduction by the 7TM region.

Greater pulling forces can lead to dissociation of the ECR, which triggers the TA-activation mechanism. Binding partners can also push on the ECR and activate the receptor by shifting the ECR conformation.

physiological contexts will shed light on this fascinating family of receptors.

Methods

Protein expression and purification

ADGRL3 protein constructs (ADGRL3 isoform 4; UniProtID: Q9HAR2-4) were expressed using the baculovirus method. *Spodoptera frugiperda* Sf9 cells (Thermo Fisher, 11496015) were transfected with specific plasmid and linearized baculovirus DNA (Expression Systems, 91-002) using Cellfectin II (Thermo Fisher, 10362100). Then, baculovirus was amplified in Sf9 cells in SF-900 III medium supplemented with 10% FBS (Sigma–Aldrich, F0926).

A construct containing Avi-tagged HormR/GAIN domains of ADGRL3 was expressed in High Five cells (Thermo Fisher, B85502) grown in Insect-Xpress medium (Lonza, 12-730Q), as described previously[35]. Briefly, cultures were infected with HormR/GAIN baculovirus at a density of 2.0×10^6 cells ml^{-1} and incubated for 72 h at 27 °C. The cells were pelleted by centrifugation, and the conditioned medium containing the secreted glycosylated proteins were collected. Final concentrations of 50 mM Tris pH 8, 5 mM CaCl$_2$, and 1 mM NiCl$_2$ were added to the media and stirred for 30 min. Formed precipitation was then removed by centrifugation at 8000×*g* for 30 min. The clear supernatant was later incubated with Ni-NTA resin (Qiagen, 30250) for 3 h. Nickel beads were collected using a glass Buchner funnel connected to a vacuum trap and washed with 10 mM HEPES pH 7.2, 150 mM NaCl, and 20 mM imidazole. HormR/GAIN domains were then biotinylated on-column with 50 mM bicine pH 8.3, 10 mM MgOAc, 100 mM NaCl, 10 mM ATP, 0.5 mM biotin, and 5 mM BirA at 27 °C with gentle mixing. The protein was eluted from the resin with 10 mM HEPES pH 7.2, 150 mM NaCl, and 200 mM imidazole, and the concentrated elution was injected onto Superdex S200 10/300 GL column (GE Healthcare) equilibrated with 10 mM HEPES; pH 7.2, 150 mM NaCl. Purified fractions of the complex were used for further experiments.

The HormR+GAIN/7TM construct of ADGRL3 was expressed in Sf9 insect cells grown in ESF 921 serum-free media (Expression System).

Cells grown to a density of 4.0×10^6 cells ml^{-1} were infected with high-titer baculovirus. Cultures were grown at 27 °C and harvested by centrifugation 50 h post infection. Cells were lysed in 10 mM Tris pH 7.5, 1 mM EDTA, and 2 mg ml^{-1} iodoacetamide supplemented with cOmplete Protease Inhibitor Cocktail tablets (Roche) in Dounce homogenizer. Membrane fractions were collected by centrifugation at 30,000×*g* at 4 °C for 1 h, and solubilized in buffer containing 30 mM HEPES pH 7.5, 500 mM NaCl, 10% glycerol, 1% (w/v) *n*-decyl-β-D-maltopyranoside (DM, Anatrace), 0.2% (w/v) cholesteryl hemisuccinate (CHS), 2 mg ml^{-1} iodoacetamide supplemented with Complete Protease Inhibitor Cocktail tablets (Roche) for 1 h at 4 °C. Cellular debris was removed by centrifugation at 100,000 *g* for 1 hour and the solubilized proteins were purified from the supernatant over M1 anti-Flag affinity resin in the presence of 2 mM CaCl$_2$. The resin was washed with 10 column volumes of 30 mM HEPES pH 7.5, 150 mM NaCl, 0.01% lauryl maltose neopentyl glycol (LMNG, Anantrace), 0.005% (w/v) CHS, 2 mM CaCl$_2$ before bound material was eluted in buffer containing 30 mM HEPES pH 7.5, 150 mM NaCl, 0.01% LMNG, 0.0025% (w/v) GDN, 8 mM EDTA and 0.2 mg ml^{-1} Flag peptide. The purified receptor was subsequently concentrated using an Amicon Ultra Centrifugal Filter (MWCO 100 kDa) and run on size-exclusion chromatography on a Superdex 200 10/300 column (GE Healthcare) pre-equilibrated with 30 mM HEPES pH 7.5, 150 mM NaCl, 0.00075% (w/v) LMNG, 0.00025% (w/v) GDN, 0.001% (w/v) CHS. Eluted fractions of the receptor were pooled and concentrated. The final yield of purified ADGRL3 was approximately 2.5 mg l^{-1} of insect cell culture.

Negative-stain electron microscopy analysis

The purified receptor was diluted to ~5 ug mL^{-1} and applied to a freshly glow-discharged EM carbon-coated copper grid (Electron Microscopy Sciences, CF400-Cu,) for 30 s. The protein was blotted off with filter paper (Sigma–Aldrich, WHA1001110), and immediately after blotting, the grid was then touched to a 25 µL drop of 1% uranyl formate solution for 30 s and blotted off, followed by air drying. The negatively-stained sample was imaged at RT with a Tecnai G2 F30 operated at 300 kV.

Images were recorded at a magnification of 49,000x and processed using EMAN2 software[83].

Phage display selection

Phage display selection for the HormR/GAIN fragment of ADGRL3 was performed according to previously published protocols[57,84]. For the first round of selection, 200 nM of protein was immobilized on streptavidin magnetic beads. The beads were washed three times to remove unbound target protein. Next, to prevent nonspecific binding of the phage, 5 mM D-biotin was added to block unoccupied streptavidin on the beads. Then, the beads were incubated for 30 min at RT with the phage library E[85], containing 10^{12}–10^{13} virions ml^{-1} with gentle shaking and washed to remove unbound phages. Beads with bound phages were used directly to infect log phase *E. coli* XL1-Blue cells. Cells were grown overnight in 2YT media with 50 µg/mL ampicillin and 10^9 p.f.u. ml^{-1} of M13 KO7 helper phage in order to amplify phages. Three additional rounds of selection were performed with decreasing target concentration in each round (100, 50, and 10 nM) using the amplified pool of virions of the prior round used as the input. Those rounds were performed using a semi-automated system with the Kingfisher instrument. In rounds 2 to 4, phages were eluted using 0.1 M glycine pH 2.7.

Enzyme-linked immunoabsorbent assays (ELISA)

ELISA experiments were carried out using a 96-well flat-bottom plate coated with 50 µL of 2 mg ml^{-1} neutravidin in Na_2CO_3 pH 9.6 and subsequently blocked with 0.5% bovine serum albumin in 1×PBS. Binding screens of all of the selected sABs in phage format was performed using a single-point phage ELISA. About 400 µL of 2YT media with 100 µg ml^{-1} ampicillin and M13 KO7 helper phage were inoculated with single *E. coli* XL1-Blue colonies harboring phagemids, and cultures were grown at 37 °C for 18 h in a 96-deep-well block plate. The cells were pelleted by centrifugation, and sAB phage-containing supernatants were diluted 20× in ELISA buffer. Diluted phages were then applied to ELISA plates and preincubated for 15 min with 50 nM of biotinylated target proteins at RT. Plates with added phages were incubated for 15 min at RT and washed three times with 1×PBST. The washing step was followed by 30 min incubation with HRP-conjugated Mouse Anti-M13 monoclonal antibody (GE Healthcare, 27942101) diluted in PBST in 1:5000 ratio. Excess antibody was washed away with 1×PBST and plates were developed using TMB substrate, quenched with 1.0 M HCl, and the signal was determined by absorbance measurement (A_{450}).

Cloning, overexpression, and purification of sABs

Phage ELISA results were used to select sAB clones that were sequenced at DNA Sequencing Facility at The University of Chicago. In-fusion cloning[86] was used to reformat unique sABs clones into pRH2.2, an IPTG inducible vector for bacterial expression.

E. coli BL21 (Gold) cells were transformed with sequence-verified sAB plasmids. Cultures were grown in 2YT media supplemented with 100 µg mL^{-1} at 37 °C until they reached OD_{600} = 0.8, when they were induced with 1 mM IPTG. The culture was continued for 4.5 h at 37 °C and cells were harvested by centrifugation. Cell pellets were resuspended in 20 mM HEPES pH = 7.5, 200 mM NaCl, 1 mM PMSF, 1 µg ml^{-1} DNase I, and lysed by ultrasonication. The cell lysate was incubated at 60 °C for 30 min. The heat-treated lysate was centrifuged at 50,000×*g* to remove cellular debris, filtered through a 0.22-µm filter, and loaded onto a HiTrap protein L (GE Healthcare) column pre-equilibrated with 20 mM HEPES pH 7.5 and 500 mM NaCl. The column was washed with 20 mM HEPES pH 7.5, and 500 mM NaCl and sABs were eluted with 0.1 M acetic acid. Protein-containing fractions were loaded directly onto an ion-exchange Resource S column pre-equilibrated with 50 mM NaOAc pH 5.0 and washed with the equilibration buffer. sABs elution was performed with a linear gradient of 0–50% of 50 mM NaOAc pH 5.0

with 2 M NaCl. Purified sABs were dialyzed overnight against 20 mM HEPES pH 7.5 with 150 mM NaCl. The quality of purified sABs was analyzed by SDS-PAGE.

Formation of receptor/sAB complex

The receptor/sAB complex was formed by mixing a 1.5-fold molar excess of the sAB with the receptor and 30 min incubation on ice. The complex was subjected to SEC on a Superdex 200 10/300 column pre-equilibrated with 30 mM HEPES pH 7.5, 150 mM NaCl, 0.00075% (w/v) LMNG, 0.00025% (w/v) GDN, 0.001% (w/v) CHS. Formation of the complex was determined by retention volume analysis of the complex with respect to that of the target alone and co-elution of the individual components on SDS-PAGE.

Cryo-EM data acquisition

For cryo-EM analysis, the purified 7TM ADGRL3/sAB complex was concentrated at 2.5 mg ml^{-1}. Right before sample processing, fluorinated octyl maltoside (FOM) was added to the solution to a final concentration of 0.05%. A vitrified specimen was prepared by applying either 3 µl of ADGRL3/LK3 complex complexes onto a glow-discharged 300 mesh gold holey carbon Quantifoil R1.2/1.3 grid (Quantifoil Micro Tools) or 2.5 µl of ADGRL3/LK1 onto a glow-discharged 300 mesh copper holey carbon Quantifoil R1.2/1.3 grid (Quantifoil Micro Tools), and frozen in liquid ethane cooled by liquid nitrogen inside a Vitrobot Mark IV (FEI). Cryo-EM imaging was performed using a Titan Krios electron microscope operated at 300 kV (Thermo Scientific) equipped with a K3 direct electron detector (Gatan, Inc.). For the ADGRL3/LK3 complex movies were recorded with a nominal magnification of ×64,000 in super-resolution counting mode, corresponding to a pixel size of 0.67 Å on the specimen level. About 6976 movies were recorded with defocus values in the range of −1.0 to −2.0 µm, using an accumulated dose rate of 65 electrons per Å^2 and a total of 58 frames per movie stack. For the ADGRL3/LK1 complex movies were recorded with a nominal magnification of ×81,000 in super-resolution counting mode, corresponding to a pixel size of 0.561 Å on the specimen level. 6210 movies were recorded with defocus values in the range of −1.4 to −2.4 µm, using an accumulated dose rate of 50.7 electrons per Å^2 and a total of 50 frames per movie stack.

Cryo-EM data processing and 3D reconstructions

ADGRL3/LK3 movies were imported to CryoSPARC 4.4[62] and stack images were subjected to full-frame and local motion correction, as well as contrast transfer function (CTF) estimation. In total, 2,621,532 particles were selected using automated particle picking. Multiple rounds of reference-free 2D classification were performed in order to discard particles grouped in poorly defined classes, resulting in 549,473 particles with well-defined features for the detergent micelle, ECR, and sAB for further processing. 3D ab initio reconstruction (with three classes) generated the initial reference maps and heterogeneous refinement, followed by non-uniform refinement was used to further classify particles and refine structures. In total, 242,439 particles from the best 3D map were then used for 3D Variability analysis[61], and separated frames from this analysis were subjected to two rounds of Heterogenous Refinement. Then, classes were subjected to iterative rounds of non-uniform refinement, with the best class accommodating 96,958 particles generating a map with an indicated global resolution of 5.5 Å. To further improve the quality of the extracellular domains in the structure, the 5.5 Å map of the entire complex was used in the local refinement job, utilizing a mask focusing on the HormR + GAIN + sAB fragment. Multiple rounds of non-uniform and local refinements produced a higher-resolution map with a global resolution of 3.9 Å. The detailed data processing flow is shown in Supplementary Fig. 2. Reported resolutions are based on the gold-standard Fourier shell correlation (FSC) using the 0.143 criterion. Local resolution was determined using half-reconstructions as input maps.

For ADGRL3/LK1, RELION 4.0 was used for the initial steps of data processing. Movies were imported and subjected to beam-induced motion correction using MotionCor2 and binned to 1.12 Å/pixel[87]. CTF parameters for each micrograph were determined by CTFFIND4[88]. About 670,000 particles were selected using automated particle picking and subjected to rounds of reference-free 2D classification to discard bad particles, resulting in 290,000 particles with well-defined features for the detergent micelle, ECR and sAB for further processing. Ab nitio model was generated, and the initial 3D maximum-likelihood-based classification was performed. About 120,000 particles from the best class were subjected to another round of 3D classification, with a total of 51,000 particles contributing to the map presented in Fig. 5j.

3D variability analysis
3D variability analysis was used to visualize movements between ECR and 7TM and to assess continuous flexibility between two parts of the protein. For this, 549,473 particles from the 2D classification first underwent non-uniform refinement with the best ab initio class as an input. The 3D variability job was then performed with three modes, with a filter resolution of 10 Å, using all particles and masks from the refinement job.

To generate a Supplementary Movie 2, a 3D variability display job was used in simple output mode with 20 frames, and visualized as a volume series in UCSF Chimera. Then, the cluster output mode of the 3D variability display job was run with five clusters. The particles and maps from each cluster were subjected to homogeneous refinement to generate the maps corresponding to the first, middle and last frames of 3D Variability analysis for a better display of the relative orientation of ECR to 7TM/micelle.

Model building and refinement
The AlphaFold2 predictions of HormR/GAIN of ADGRL3 and sAB LK3 were used for model building[60]. Models were manually fitted into the density map of HormR + GAIN/LK3 using the Fit in Map function of UCSF ChimeraX[89]. Then, the model was docked into the EM density map using the Phenix dock in map function, refined using the real-space refinement module in the Phenix software suite[90], and then manually checked and adjusted residue-by-residue to fit the density using COOT[91], in an iterative manner. Structural figures were created using UCSF ChimeraX[89].

Serum response element luciferase assays
HEK293T cells (ATCC, CRL-3216) were seeded on a 96-well flat-bottom plate precoated with 0.5% gelatin and grown until 50–60% confluent in DMEM supplemented with 10% (v/v) FBS at 37 °C and 5% CO_2. Cells were then co-transfected with full-length ADGRL3 (1 ng well^{-1})[24,35], Dual-Glo luciferase reporter plasmid (20 ng well^{-1})[34], using 0.3 µL LipoD293T (SL100668; SignaGen Laboratories). DNA levels were balanced among transfections by the addition of the empty pCMV5 vector to 100 ng total DNA. Eighteen hours after transfection media was aspirated and replaced with DMEM without FBS. When sABs were tested, 1 µM of sAB was added 5 h after the start of the serum-starvation. After 10 h of serum starvation, cells were lysed using the Dual-Glo Luciferase Assay System from Promega, and firefly and renilla luciferase signals were measured using a Synergy HTX (BioTek) luminescence plate reader. The firefly:renilla ratio for each well was calculated and normalized to an empty vector. Data were then analyzed using GraphPad Prism 9.3.1 software and presented as mean ± SD of three repeats ($n = 3$) for a representative of three independent experiments.

cAMP assay
HEK293 cells (ATCC CRL-1573) were seeded in six-well plates with DMEM supplemented with 10% (v/v) FBS at 37 °C and 5% CO_2. After ~24 h, when cells reached 50–60% confluence, they were transfected with 350 ng of ADGRL3 + 350 ng 22 F Glosensor reporter plasmid (E2301; Promega) + 9 ng of β2-adrenergic receptor + 2.8 uL of transfection reagent Fugene 6 (Promega, PRE2693). The next day, cells were detached with trypsin and seeded at 5×10^4 per well in a white flat-bottom 96-well plate. After another 24 h, the complete media was replaced with 100 ul Opti-MEM I Reduced-Serum Medium (31985070, Life Technologies) and incubated for 30 min. Then, 1 uL Glosensor substrate and 11 uL FBS were added to each well. The basal cAMP signal was measured after 20 min of equilibration time. When sABs were tested, cells were treated with 1 uM of sAB for 5 min and then activated with 50 nM isoproterenol. Measurements were done using Synergy HTX BioTek plate reader at 25 °C. Data were then analyzed using GraphPad Prism 9.3.1 software and presented as mean ± SD.

Molecular cloning of smFRET constructs
The C-terminal eGFP-tagged human ADGRL3 construct was cloned in pcDNA3.1(+) vector with 12 amino acids linker and verified by sequencing (ACGT Inc). Full-length ADGRL3 constructs with an amber codon (TAG) mutation of amino acid Y795 and A871, R933, or E1099, as well as variants harboring cancer mutations S810L/E811Q were generated with QuickChange site-directed mutagenesis (Agilent). All constructs were verified with full-length sequencing (Primordium Labs). DNA restriction enzymes, DNA polymerase, and DNA ligase were from New England Biolabs. Plasmid preparation kits were purchased from Macherey-Nagel.

Transfection and protein expression for smFRET experiments
HEK293T cells (Sigma) were maintained in DMEM (Gibco) supplemented with 10% (v/v) serum (Cytiva), 100 unit/mL penicillin-streptomycin (Gibco) and 15 mM HEPES (pH = 7.4, Gibco) at 37 °C and 5% CO_2. The cells were passaged with 0.05% trypsin-EDTA (Gibco). For unnatural amino acid-containing protein expression, the growth media was supplemented with 0.25 mM trans-cyclooct-2-en – ʟ – lysine (SiChem, #SC-8008). All media was filtered by a 0.2 µM PES filter (Fisher Scientific).

Twenty-four hours before transfection, HEK293T cells were cultured on poly-ʟ-lysine-coated 18 mm glass coverslips (VWR) at 60–70% confluency. Two hours before transfection, the media was changed to the growth media supplemented with 0.25 mM trans-cyclooct-2-en – ʟ – lysine ADGRL3 plasmids with amber codon and pNEU-hMbPylRS-4xU6M15 (pNEU-hMbPylRS-4xU6M15 was a gift from Irene Coin, Addgene plasmid # 105830) were co-transfected (1:1 w/w) into cells using Lipofectamine 3000 (Fisher Scientific) (total plasmid: 2 µg/18 mm coverslip). After 48 h supplemented growth media was removed and cells were washed by extracellular buffer solution containing (in mM): 128 NaCl, 2 KCl, 2.5 CaCl$_2$, 1.2 MgCl$_2$, 10 sucrose, 10 HEPES, pH = 7.4 and were kept in growth medium without trans-cyclooct-2-en – ʟ – lysine for 30 min. Site-specific labeling with Cy3 and Cy5 fluorophores was done by diluting Cy3 and Cy5 alkyne dyes (Click Chemistry Tools) to the final concentration of 40 µM each in the extracellular buffer and incubating for 15 min in the incubator. After labeling, coverslips were gently washed by the extracellular buffer solution to remove excess dye. Live-cell images of labeled cells were collected using a Zeiss LSM800 confocal microscope with a Plan-Apochromat ×40 objective (Zeiss, 1.3 numerical aperture, oil immersion) and Zen Blue software.

Single-molecule FRET measurements
Single-molecule experiments were conducted in chambers prepared from glass coverslips (VWR), and microscope slides (Fisher Scientific) passivated with mPEG (Laysan Bio) and biotin-PEG as previously described[67]. Prior to experiments, flow cells were functionalized with NeutrAvidin (Fisher Scientific) and anti-GFP antibody (Abcam, #ab6658).

After labeling, cells were incubated in DPBS without Ca^{2+}/Mg^{2+} for 15 min and harvested. Afterward, cells were resuspended in 100 µL lysis buffer consisting of 200 mM NaCl, 50 mM HEPES, 1 mM EDTA,

protease inhibitor tablet (Fisher Scientific), and 0.1 w/v% LMNG-CHS (10:1, Anatrace), pH 7.4. Cells were lysed with gentle mixing at 4 °C for 1 h. The cell lysate was then centrifuged for 20 min at 20,000×g and 4 °C. The supernatant was collected and kept on ice. Diluted cell lysate was immobilized in the imaging chamber and imaged in an imaging buffer consisting of (in mM) 128 NaCl, 2 KCl, 2.5 CaCl$_2$, 1.2 MgCl$_2$, 40 HEPES, 4 Trolox, 0.005 w/v% LMNG-CHS (10:1), 0.0004 w/v% GDN, and an oxygen scavenging system consisting of protocatechuic acid (Sigma) and 1.6 U/mL bacterial protocatechuate 3,4-dioxygenase (rPCO) (Oriental Yeast Co.), pH 7.35. Samples were imaged with a 100× objective (Olympus, 1.49 NA, Oil immersion) on a custom-built microscope with 30 ms time resolution unless stated otherwise. 532 nm and 638 nm lasers (RPMC Lasers) were used for donor and acceptor excitation, respectively.

smFRET data analysis

Analysis of single-molecule fluorescence data was performed as described before[66]. Particles that showed an acceptor signal upon donor excitation with acceptor intensity greater than 10% above background, were automatically selected, and donor and acceptor intensities were measured over all frames. Out of this pool (400–600 total), particles that showed a single donor and a single acceptor bleaching step during the acquisition time, showed stable total intensity ($I_D + I_A$), anti-correlated donor and acceptor intensity behavior without blinking events, and lasted at least 4 seconds before bleaching were manually selected for further analysis (~20–30% of total molecules per movie). A subset of the data were analyzed by two individuals independently, and the results were compared and shown to be identical. FRET efficiency was calculated as ($I_A - 0.085 \times I_D$)/($I_D + (I_A - 0.085 \times I_D$)), where I_D and I_A are raw donor and acceptor intensities, respectively. Data were not corrected for the direct excitation of the acceptor by a 532 nm laser. Data were collected for at least three independent biological replicates, and the results were averaged. Population smFRET histograms were generated by compiling at least 250 total FRET traces of molecules from all replicates. To ensure that each trace contributes equally, the area under the FRET histogram of individual molecules was normalized to one. Error bars on histograms represent the standard error of the mean of data. We used the same imaging parameters, including the laser intensity, data acquisition rate, and buffer composition between different samples, and all the data were treated the same for analysis. To avoid bias from very short traces, only data that is longer than 5 s is kept for final analysis.

A hidden Markov model (HMM) using vbFRET software was used to idealize FRET traces[92,93] and generate the transition density plots with number of states set to one to five states. TDP plots for each replicate showed three definitive FRET states. This was also corroborated with manual inspection of all the traces.

Next, peak fitting analysis on population smFRET histograms was performed with OriginPro and used three Gaussian distributions as

$$y(x) = \sum_{i=1}^{3} \frac{A_i}{w_i \sqrt{\frac{\pi}{2}}} e^{-2\frac{(x-xc_i)^2}{w_i^2}},$$ where A is the peak area, w is the peak width, and xc is the peak center. Peak areas were constrained to A > 0. Peak widths were constrained to 0.1 < w < 0.17. Peak centers were constrained to ±0.02 of the mean FRET efficiency of each FRET state obtained from the TDP plots.

Reporting summary

Further information on research design is available in the Nature Portfolio Reporting Summary linked to this article.

Data availability

The cryo-EM density map has been deposited in the Electron Microscopy Data Bank under accession code EMD-43523, and the coordinates for the model of HormR/GAIN domains of ADGRL3 in complex with sAB LK3 generated in this study have been deposited in the Protein Data Bank under accession code PDB 8vti. The available structure of the apo-state 7TM region of ADGRL3 referenced in this work is available under the accession code 8jmt. Sample single molecule image data of ADGRL3 WT and ADGRL3 S810L/E811Q has been deposited in the Harvard Dataverse repository at https://doi.org/10.7910/DVN/W446VI. All data supporting the findings of this study are available within the article and Supplementary Information/Source Data files. Raw smFRET traces data sets can be provided upon request to the corresponding author R.V. Source data are provided with this paper.

References

1. Folts, C. J., Giera, S., Li, T. & Piao, X. Adhesion G protein-coupled receptors as drug targets for neurological diseases. *Trends Pharmacol. Sci.* **40**, 278–293 (2019).
2. Monk, K. R. et al. Adhesion G protein-coupled receptors: from in vitro pharmacology to in vivo mechanisms. *Mol. Pharmacol.* **88**, 617–623 (2015).
3. Araç, D. & Leon, K. in *GPCRs Structure Function and Drug Discovery* (Elsevier, 2020).
4. Bae, B.-I. et al. Evolutionarily dynamic alternative splicing of GPR56 regulates regional cerebral cortical patterning. *Science* **343**, 764–768 (2014).
5. Pederick, D. T. et al. Reciprocal repulsions instruct the precise assembly of parallel hippocampal networks. *Science* **372**, 1068–1073 (2021).
6. Piao, X. et al. G protein-coupled receptor-dependent development of human frontal cortex. *Science* **303**, 2033–2036 (2004).
7. Sando, R., Jiang, X. & Südhof, T. C. Latrophilin GPCRs direct synapse specificity by coincident binding of FLRTs and teneurins. *Science* **363**, eaav7969 (2019).
8. Wang, J. et al. RTN4/NoGo-receptor binding to BAI adhesion-GPCRs regulates neuronal development. *Cell* **185**, 218 (2022).
9. Monk, K. R. et al. A G protein-coupled receptor is essential for Schwann cells to initiate myelination. *Science* **325**, 1402–1405 (2009).
10. Kuhnert, F. et al. Essential regulation of CNS angiogenesis by the orphan G protein-coupled receptor GPR124. *Science* **330**, 985–989 (2010).
11. Langenhan, T. et al. Latrophilin signaling links anterior-posterior tissue polarity and oriented cell divisions in the C. elegans embryo. *Dev. Cell* **17**, 494–504 (2009).
12. Usui, T. et al. Flamingo, a seven-pass transmembrane cadherin, regulates planar cell polarity under the control of Frizzled. *Cell* **98**, 585–595 (1999).
13. Langenhan, T., Aust, G. & Hamann, J. Sticky signaling–adhesion class G protein-coupled receptors take the stage. *Sci. Signal.* **6**, re3–re3 (2013).
14. Liebscher, I. et al. A guide to adhesion GPCR research. *FEBS J.* **289**, 7610–7630 (2021).
15. O'Hayre, M. et al. The emerging mutational landscape of G proteins and G-protein-coupled receptors in cancer. *Nat. Rev. Cancer* **13**, 412–424 (2013).
16. Prömel, S., Langenhan, T. & Araç, D. Matching structure with function: the GAIN domain of Adhesion-GPCR and PKD1-like proteins. *Trends Pharmacol. Sci.* **34**, 470–478 (2013).
17. Drews, J. Drug discovery: a historical perspective. *Science* **287**, 1960–1964 (2000).
18. Lala, T. & Hall, R. A. Adhesion G protein-coupled receptors: structure, signaling, physiology, and pathophysiology. *Physiol. Rev.* **102**, 1587–1624 (2022).
19. Araç, D. et al. A novel evolutionarily conserved domain of cell-adhesion GPCRs mediates autoproteolysis. *EMBO J.* **31**, 1364–1378 (2012).

20. Chang, G.-W. et al. Proteolytic cleavage of the EMR2 receptor requires both the extracellular stalk and the GPS motif. *FEBS Lett.* **547**, 145–150 (2003).

21. Lin, H.-H. et al. Autocatalytic cleavage of the EMR2 receptor occurs at a conserved G protein-coupled receptor proteolytic site motif. *J. Biol. Chem.* **279**, 31823–31832 (2004).

22. Liebscher, I. et al. A tethered agonist within the ectodomain activates the adhesion G protein-coupled receptors GPR126 and GPR133. *Cell Rep.* **9**, 2018–2026 (2014).

23. Stoveken, H. M., Hajduczok, A. G., Xu, L. & Tall, G. G. Adhesion G protein-coupled receptors are activated by exposure of a cryptic tethered agonist. *Proc. Natl Acad. Sci. USA* **112**, 6194–6199 (2015).

24. Nazarko, O. et al. A comprehensive mutagenesis screen of the adhesion GPCR latrophilin-1/ADGRL1. *iScience* **3**, 264–278 (2018).

25. Wilde, C. et al. The constitutive activity of the adhesion GPCR GPR114/ADGRG5 is mediated by its tethered agonist. *FASEB J.* **30**, 666–673 (2016).

26. Bernadyn, T. F., Vizurraga, A., Adhikari, R., Kwarcinski, F. & Tall, G. G. GPR114/ADGRG5 is activated by its tethered peptide agonist because it is a cleaved adhesion GPCR. *J. Biol. Chem.* **299**, 105223 (2023).

27. Kishore, A., Purcell, R. H., Nassiri-Toosi, Z. & Hall, R. A. Stalk-dependent and stalk-independent signaling by the adhesion G protein-coupled receptors GPR56 (ADGRG1) and BAI1 (ADGRB1). *J. Biol. Chem.* **291**, 3385–3394 (2016).

28. Salzman, G. S. et al. Stachel -independent modulation of GPR56/ADGRG1 signaling by synthetic ligands directed to its extracellular region. *Proc. Natl Acad. Sci. USA* **114**, 10095–10100 (2017).

29. Bui, D. L. H. et al. The adhesion GPCRs CELSR1–3 and LPHN3 engage G proteins via distinct activation mechanisms. *Cell Rep.* **42**, 112552 (2023).

30. Prömel, S. et al. The GPS motif is a molecular switch for bimodal activities of adhesion class G protein-coupled receptors. *Cell Rep.* **2**, 321–331 (2012).

31. Dates, A. N. et al. Heterogeneity of tethered agonist signaling in adhesion G protein-coupled receptors. *Cell Chem. Biol.* **31**, 1542–1553.e4 (2024).

32. Leon, K. et al. Structural basis for adhesion G protein-coupled receptor Gpr126 function. *Nat. Commun.* **11**, 194 (2020).

33. Purcell, R. H. & Hall, R. A. Adhesion G protein–coupled receptors as drug targets. *Annu. Rev. Pharmacol. Toxicol.* **58**, 429–449 (2018).

34. Salzman, G. S. et al. Structural basis for regulation of GPR56/ADGRG1 by its alternatively spliced extracellular domains. *Neuron* **91**, 1292–1304 (2016).

35. Kordon, S. P. et al. Isoform- and ligand-specific modulation of the adhesion GPCR ADGRL3/Latrophilin3 by a synthetic binder. *Nat. Commun.* **14**, 635 (2023).

36. Stephan, G., Frenster, J. D., Liebscher, I. & Placantonakis, D. G. Activation of the adhesion G protein-coupled receptor GPR133 by antibodies targeting its N-terminus. *J. Biol. Chem.* **298**, 101949 (2022).

37. Paavola, K. J., Stephenson, J. R., Ritter, S. L., Alter, S. P. & Hall, R. A. The N terminus of the adhesion G protein-coupled receptor GPR56 controls receptor signaling activity. *J. Biol. Chem.* **286**, 28914–28921 (2011).

38. Beliu, G. et al. Tethered agonist exposure in intact adhesion/class B2 GPCRs through intrinsic structural flexibility of the GAIN domain. *Mol. Cell* **81**, 905–921.e5 (2021).

39. Barros-Álvarez, X. et al. The tethered peptide activation mechanism of adhesion GPCRs. *Nature* **604**, 757–762 (2022).

40. Xiao, P. et al. Tethered peptide activation mechanism of the adhesion GPCRs ADGRG2 and ADGRG4. *Nature* **604**, 771–778 (2022).

41. Ping, Y.-Q. et al. Structural basis for the tethered peptide activation of adhesion GPCRs. *Nature* **604**, 763–770 (2022).

42. Qu, X. et al. Structural basis of tethered agonism of the adhesion GPCRs ADGRD1 and ADGRF1. *Nature* **604**, 779–785 (2022).

43. Ohta, S. et al. Agonistic antibodies reveal the function of GPR56 in human glioma U87-MG cells. *Biol. Pharm. Bull.* **38**, 594–600 (2015).

44. Chu, T.-Y. et al. GPR97 triggers inflammatory processes in human neutrophils via a macromolecular complex upstream of PAR2 activation. *Nat. Commun.* **13**, 6385 (2022).

45. Wang, F. et al. Crystal structure of the extracellular domains of GPR110. *J. Mol. Biol.* **435**, 167979 (2023).

46. Guo, Q. et al. A method for structure determination of GPCRs in various states. *Nat. Chem. Biol.* **20**, 74–82 (2024).

47. Moreno-Salinas, A. L. et al. Latrophilins: a neuro-centric view of an evolutionary conserved adhesion G protein-coupled receptor subfamily. *Front. Neurosci.* **13**, 700 (2019).

48. Mathiasen, S. et al. G12/13 is activated by acute tethered agonist exposure in the adhesion GPCR ADGRL3. *Nat. Chem. Biol.* **16**, 1343–1350 (2020).

49. Qian, Y. et al. Structural insights into adhesion GPCR ADGRL3 activation and Gq, Gs, Gi, and G12 coupling. *Mol. Cell* **82**, 4340–4352.e6 (2022).

50. Wang, S. et al. Alternative splicing of latrophilin-3 controls synapse formation. *Nature* **626**, 128–135 (2024).

51. Arcos-Burgos, M. et al. A common variant of the latrophilin 3 gene, LPHN3, confers susceptibility to ADHD and predicts effectiveness of stimulant medication. *Mol. Psychiatry* **15**, 1053–1066 (2010).

52. Jain, M. et al. A cooperative interaction between LPHN3 and 11q doubles the risk for ADHD. *Mol. Psychiatry* **17**, 741–747 (2012).

53. Sando, R. & Südhof, T. C. Latrophilin GPCR signaling mediates synapse formation. *Elife* **10**, e65717 (2021).

54. Li, J. et al. Alternative splicing controls teneurin-latrophilin interaction and synapse specificity by a shape-shifting mechanism. *Nat. Commun.* **11**, 2140 (2020).

55. del Toro, D. et al. Structural basis of teneurin-latrophilin interaction in repulsive guidance of migrating neurons. *Cell* **180**, 323–339.e19 (2020).

56. Perry-Hauser, N. A., VanDyck, M. W., Lee, K. H., Shi, L. & Javitch, J. A. Disentangling autoproteolytic cleavage from tethered agonist–dependent activation of the adhesion receptor ADGRL3. *J. Biol. Chem.* **298**, 102594 (2022).

57. Paduch, M. et al. Generating conformation-specific synthetic antibodies to trap proteins in selected functional states. *Methods* **60**, 3–14 (2013).

58. Dutka, P. et al. Development of "plug and play" fiducial marks for structural studies of GPCR signaling complexes by single-particle cryo-EM. *Structure* **27**, 1862–1874.e7 (2019).

59. Mukherjee, S. et al. Synthetic antibodies against BRIL as universal fiducial marks for single–particle cryoEM structure determination of membrane proteins. *Nat. Commun.* **11**, 1598 (2020).

60. Mirdita, M. et al. ColabFold: making protein folding accessible to all. *Nat. Methods* **19**, 679–682 (2022).

61. Punjani, A. & Fleet, D. J. 3D variability analysis: resolving continuous flexibility and discrete heterogeneity from single particle cryo-EM. *J. Struct. Biol.* **213**, 107702 (2021).

62. Punjani, A., Rubinstein, J. L., Fleet, D. J. & Brubaker, M. A. cryoSPARC: algorithms for rapid unsupervised cryo-EM structure determination. *Nat. Methods* **14**, 290–296 (2017).

63. Kaszuba, K. et al. N -Glycosylation as determinant of epidermal growth factor receptor conformation in membranes. *Proc. Natl Acad. Sci. USA* **112**, 4334–4339 (2015).

64. Faust, B. et al. Autoantibody mimicry of hormone action at the thyrotropin receptor. *Nature* **609**, 846–853 (2022).

65. Polley, A. et al. Glycosylation and lipids working in concert direct CD2 ectodomain orientation and presentation. *J. Phys. Chem. Lett.* **8**, 1060–1066 (2017).

66. Liauw, B. W.-H., Afsari, H. S. & Vafabakhsh, R. Conformational rearrangement during activation of a metabotropic glutamate receptor. *Nat. Chem. Biol.* **17**, 291–297 (2021).

67. Liauw, B. W.-H. et al. Conformational fingerprinting of allosteric modulators in metabotropic glutamate receptor 2. *Elife* **11**, e78982 (2022).

68. Schamber, M. R. & Vafabakhsh, R. Mechanism of sensitivity modulation in the calcium-sensing receptor via electrostatic tuning. *Nat. Commun.* **13**, 2194 (2022).

69. Bhudia, N. et al. G protein-coupling of adhesion GPCRs ADGRE2/EMR2 and ADGRE5/CD97, and activation of G protein signalling by an anti-EMR2 antibody. *Sci. Rep.* **10**, 1004 (2020).

70. Chatterjee, T. et al. Anti-GPR56 monoclonal antibody potentiates GPR56-mediated Src-Fak signaling to modulate cell adhesion. *J. Biol. Chem.* **296**, 100261 (2021).

71. Avila-Zozaya, M., Rodríguez-Hernández, B., Monterrubio-Ledezma, F., Cisneros, B. & Boucard, A. A. Thwarting of Lphn3 functions in cell motility and signaling by cancer-related GAIN domain somatic mutations. *Cells* **11**, 1913 (2022).

72. Vizurraga, A., Adhikari, R., Yeung, J., Yu, M. & Tall, G. G. Mechanisms of adhesion G protein–coupled receptor activation. *J. Biol. Chem.* **295**, 14065–14083 (2020).

73. Zhong, B. L. et al. Piconewton forces mediate GAIN domain dissociation of the latrophilin-3 adhesion GPCR. *Nano Lett.* **23**, 9187–9194 (2023).

74. Dumas, L. et al. Uncovering and engineering the mechanical properties of the adhesion GPCR ADGRG1 GAIN domain. Preprint at *bioRxiv* (2023).

75. Pan, J. et al. Quantifying molecular- to cellular-level forces in living cells. *J. Phys. D. Appl. Phys.* **54**, 483001 (2021).

76. Pfreundschuh, M. et al. Identifying and quantifying two ligand-binding sites while imaging native human membrane receptors by AFM. *Nat. Commun.* **6**, 8857 (2015).

77. Alsteens, D. et al. Nanomechanical mapping of first binding steps of a virus to animal cells. *Nat. Nanotechnol.* **12**, 177–183 (2017).

78. Ott, W., Jobst, M. A., Schoeler, C., Gaub, H. E. & Nash, M. A. Single-molecule force spectroscopy on polyproteins and receptor–ligand complexes: the current toolbox. *J. Struct. Biol.* **197**, 3–12 (2017).

79. Cukierman, E., Pankov, R., Stevens, D. R. & Yamada, K. M. Taking cell-matrix adhesions to the third dimension. *Science* **294**, 1708–1712 (2001).

80. Geiger, B. & Bershadsky, A. Exploring the neighborhood: adhesion-coupled cell mechanosensors. *Cell* **110**, 139–142 (2002).

81. Bershadsky, A. D., Balaban, N. Q. & Geiger, B. Adhesion-dependent cell mechanosensitivity. *Annu. Rev. Cell Dev. Biol.* **19**, 677–695 (2003).

82. Bandekar, S. J. et al. Structure of the extracellular region of the adhesion GPCR CELSR1 reveals a compact module which regulates G protein-coupling. Preprint at *bioRxiv* (2024).

83. Tang, G. et al. EMAN2: an extensible image processing suite for electron microscopy. *J. Struct. Biol.* **157**, 38–46 (2007).

84. Fellouse, F. A. et al. High-throughput generation of synthetic antibodies from highly functional minimalist phage-displayed libraries. *J. Mol. Biol.* **373**, 924–940 (2007).

85. Miller, K. R. et al. T cell receptor-like recognition of tumor in vivo by synthetic antibody fragment. *PLoS ONE* **7**, e43746 (2012).

86. Raman, M. & Martin, K. One solution for cloning and mutagenesis: In-Fusion® HD Cloning Plus. *Nat. Methods* **11**, iii–v (2014).

87. Zheng, S. Q. et al. MotionCor2: anisotropic correction of beam-induced motion for improved cryo-electron microscopy. *Nat. Methods* **14**, 331–332 (2017).

88. Rohou, A. & Grigorieff, N. CTFFIND4: fast and accurate defocus estimation from electron micrographs. *J. Struct. Biol.* **192**, 216–221 (2015).

89. Pettersen, E. F. et al. UCSF chimeraX: structure visualization for researchers, educators, and developers. *Protein Sci.* **30**, 70–82 (2021).

90. Liebschner, D. et al. Macromolecular structure determination using X-rays, neutrons and electrons: recent developments in Phenix. *Acta Crystallogr. Sect. D. Struct. Biol.* **75**, 861–877 (2019).

91. Emsley, P., Lohkamp, B., Scott, W. G. & Cowtan, K. Features and development of Coot. *Acta Crystallogr. Sect. D. Biol. Crystallogr.* **66**, 486–501 (2010).

92. Bronson, J. E., Fei, J., Hofman, J. M., Gonzalez, R. L. & Wiggins, C. H. Learning rates and states from biophysical time series: a Bayesian approach to model selection and single-molecule FRET data. *Biophys. J.* **97**, 3196–3205 (2009).

93. Zhang, J. et al. Specific structural elements of the T-box riboswitch drive the two-step binding of the tRNA ligand. *Elife* **7**, e39518 (2018).

Acknowledgements

Author contributions
S.P.K., K.C., R.V., and D.A. designed all experiments and interpreted results. K.C. and K.L. cloned constructs for smFRET and protein expression and purification experiments. S.P.K. expressed and purified all proteins (with assistance from K.L.), prepared EM samples, and performed specimen screening, data collection and cryo-EM data analysis. S.J.B. assisted with cryo-EM map calculation and built and refined the HormR/GAIN structure. K.C. prepared smFRET specimens and performed smFRET measurements (with assistance from G.S.) and data analysis. P.D. carried out phage display selection and sABs characterization. S.P.K. performed cell-based signaling assays. D.A., S.P.K., R.V., and K.C. wrote the manuscript with assistance from, S.J.B and P.D. D.A., R.V., and A.A.K. supervised the project.

Competing interests
The authors declare no competing interests.

Additional information